

Article

Significance of Calcite Trace Elements Contents and C-O Isotopic Compositions for Ore-Forming Fluids and Gold Prospecting in the Zhesang Carlin-Like Gold Deposit of Southeastern Yunnan, China

Jiasheng Wang ^{1,*}, Jinyang Chang ¹, Chao Li ², Zhenchun Han ³, Tao Wang ⁴ and Huanhuan Han ¹

¹ Southwest Institute of Geological Survey; Kunming University of Science and Technology, Kunming 650093, China; CJY1992922@163.com (J.C.); H1226685364@163.com (H.H.)

² Re-Os Laboratory, National Research Center for Geoanalysis, Beijing 100037, China; Re-Os@163.com

³ 11th Geology Team of Zhejiang Province, Wenzhou 325006, China; im.hzc@outlook.com

⁴ Yunnan Institute of Geological Survey, Yunnan Geological Survey, Kunming 650011, China; wangtao_abcd@163.com

* Correspondence: jiashengwang@kust.edu.cn; Tel.: +86-0871-6518-0377

Received: 8 January 2020; Accepted: 7 April 2020; Published: 9 April 2020



Abstract: The Zhesang gold deposit of southeastern Yunnan is an important component of the Dian-Qian-Gui (Yunnan, Guizhou, and Guangxi) “Golden Triangle”, which hosts a multitude of Carlin-like gold deposits (CLGDs). Calcite is one of the most common gangue minerals in Zhesang. The calcites that have been found in the mining area are classified as ore-stage and post-ore calcites. The ore-stage calcite exhibits a clear paragenetic relationship with gold-bearing arsenopyrite and with an alteration halo that has been cut by the post-ore calcite. To elucidate the origin of the ore-forming fluids of the Zhesang gold deposit and to investigate the possibility of utilizing calcite geochemistry as prospecting indicators, the rare earth elements (REEs), Y, Fe, Mn and Mg contents, and C-O isotopic compositions of calcites from Zhesang have been analyzed. The ore-stage calcite is enriched in middle rare earth elements (MREEs) relative to light rare earth elements (LREEs) and heavy rare earth elements (HREEs) (MREE/LREE = 1.11–1.61, MREE/HREE = 6.12–8.22), whereas post-ore calcite exhibits an enrichment in LREE (LREE/HREE = 4.39–14.93, MREE/LREE = 0.35–0.71). The ore-stage and post-ore calcites were both formed by hydrothermal fluids; however, these hydrothermal fluids may have different sources. The Fe contents of the ore-stage calcite are significantly higher than those of post-ore calcite (4690–6300 µg/g versus 2030–2730 µg/g). Ore-stage calcite also has significantly lower $\delta^{18}\text{O}_{\text{V-SMOW}}$ values than post-ore calcite (11.03–12.49‰ versus 16.48–17.14‰). These calcites with an MREE/LREE ratio greater than 0.92, MREE/HREE ratio greater than 5.69, Fe content greater than 3827 µg/g, and $\delta^{18}\text{O}_{\text{V-SMOW}}$ value less than 14.40‰ represent ore-stage calcites and are important prospecting guidelines. According to the REE, C-O isotopic characteristics of the calcites and the previous findings, it is inferred that the ore-forming fluids of the Zhesang gold deposit were a mixture of crustal fluid by meteoric water leaching wall rocks and a small amount of basic magmatic fluid. The formation of post-ore calcite might be derived from meteoric water and marine carbonates interaction. The ore-forming fluids of the Zhesang gold deposit may be associated with the intrusion of diabase that outcrops in the mining area, and that the basic magmatic activities of the Indosinian period also provided some of the ore-forming materials and heat for gold mineralization.

Keywords: Zhesang Carlin-like gold deposit; calcite; trace elements; C-O isotopes; ore-forming fluids; prospecting

1. Introduction

Carlin-type gold deposits are sediment-hosted disseminated gold deposits [1,2], and they were first recognized as a new type of deposit in 1961, after the development of the Carlin Mine in Nevada, USA [2,3]. Ever since the discovery of gold deposits in Banqi (Qianxinan Prefecture, Guizhou) in the 1980s, the metallogenesis and classification of the gold deposits of the Dian-Qian-Gui region are still mired in controversy [4–10]. Most researchers accept that the gold deposits of the Dian-Qian-Gui region are Carlin-type gold deposits in consideration of the geologic setting of the Dian-Qian-Gui is similar to that of Nevada in that it includes rifting of craton, deposition of a passive sequence, and subsequent contractional deformations [4,11–13]. However, the Dian-Qian-Gui gold deposits also exhibit some significant differences with the Nevada Carlin-type gold deposits. For instance, a key difference is that there is no temporally related felsic magmatism in the Chinese gold district [7]. Another significant difference is the abundance of vein quartz and calcite in the Dian-Qian-Gui deposits, which is rare in the Nevada deposits [4]. Besides, the temperatures and pressures of mineralization are 190–300 °C and 0.45–2.3 kbar, respectively, in the Dian-Qian-Gui, while they are 180–240 °C and 0.33–0.65 kbar in the Nevada [2,4,7,14–17]. Therefore, some researchers named them Carlin-like gold deposits (CLGDs) [12]. Based on the critical similarities and differences between Dian-Qian-Gui and Nevada gold deposits, in this work, the Zhesang deposit has been classified as CLGD.

The CLGDs of southeastern Yunnan are an important component of the Dian-Qian-Gui “Golden Triangle” (Figure 1). Su et al. [7] categorized the gold deposits of this region into three types based on the host rocks, occurrence, and location of each deposit: (1) carbonate-hosted gold deposits in the northern part of Dian-Qian-Gui (e.g., the Shuiyindong deposit), (2) northern siliciclastic/fault-hosted gold deposits (e.g., the Lannigou deposit), and (3) southern diabase-hosted gold deposits (e.g., the Anna deposit). These deposit types differ in their host rocks and metallogenic/tectonic background, and the differences are especially stark between the northern and southern deposits in terms of their mineral assemblages and metallogenic features. Based on the above classification, Zhesang belongs to the type of the southern diabase-hosted gold deposit.

The origin of the ore-forming fluids of Carlin-like (-type) gold deposits is still hotly debated. Cline and Hofstra [18] proposed that the ore-forming fluids of the Carlin-type gold deposits in Nevada originated from modified water, whereas Arehart [19] and Emsbo and Hofstra [20] postulated that the ore-forming fluids of these deposits are sourced from meteoric water. On the other hand, Muntean et al. [21] concluded that the mineralization of these gold deposits is closely related to magmatic hydrothermal activity. Similarly, Hu et al. [14] hypothesized that the ore-forming fluids of the CLGD in Dian-Qian-Gui originated from meteoric water, whereas Su et al. [22] and Hofstra et al. [23] postulated that modified waters make up most of the ore-forming fluids in these deposits. Peng et al. [24] proposed that the ore-forming fluids in this region are hydrocarbon-bearing basin fluids. However, some researchers believe that the formation of CLGD in Dian-Qian-Gui is associated with mantle plumes or deep magmatic activity, as the deep, large cracks of the Youjiang Basin, which provided a path for the upwelling of deep fluids [25–27].

Zhesang gold deposit is a large gold deposit that is representative of its class of deposits, and it has been the subject of numerous studies, including studies about its mineralization epochs, gold occurrence, typomorphic minerals, fluid inclusions, and ore-forming fluids resources. Pi et al. [27] determined that the age of Zhesang gold mineralization is 215.3 ± 1.9 Ma based on hydrothermal sericite $^{40}\text{Ar}/^{39}\text{Ar}$ plateau age; this age is in accordance with the U-Pb age of 219.9 ± 6.6 Ma for the late Indosinian basic rock in the region [28], suggesting that the late Indosinian basic rock could be closely related to the gold mineralization. Zhang [29] pointed out that gold exists in the form of microscopic or submicroscopic native gold mainly in metal sulfides or metallic oxides, such as pyrite and arsenopyrite, and secondly in gangue minerals, like silicate and carbonate. Gao and Huang [30] reported that fluid inclusion homogenization temperatures of the ore-stage range from 194 to 295 °C, with salinities of 3.72 to 15.74 wt.% NaCl equiv, which belongs to medium-high temperature, medium-low salinity. Currently, the source of ore-forming fluids in Zhesang is still controversial. Pi et al. [27] and Dai et al. [31] believed

that the ore-forming fluid derived from crustal fluids. Gao and Huang [30] suggested that the Zhesang ore-forming fluid is a mixture of magmatic and meteoric waters. Wei et al. [28] proposed that the deep-seated magma triggered fluids of possibly meteoric origin to circulate and leach out ore-forming elements from sedimentary rocks to form the Zhesang gold deposit.

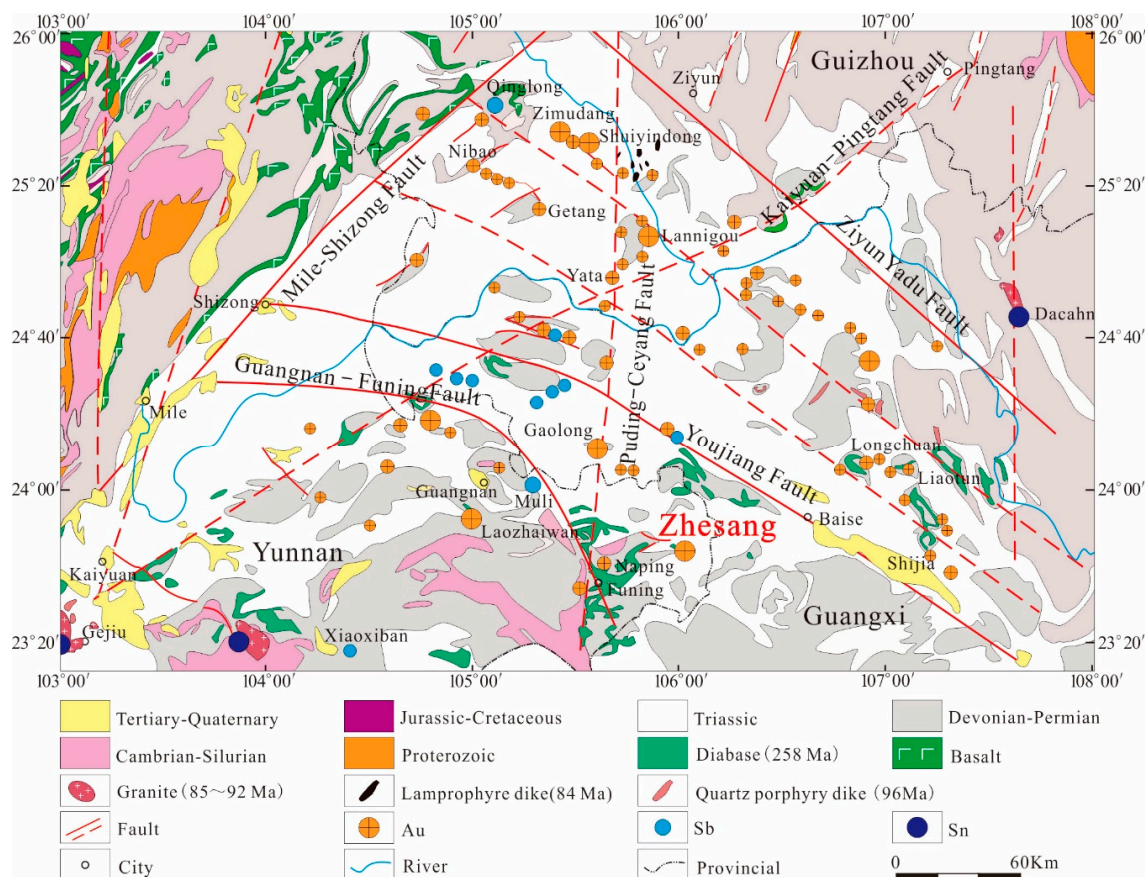


Figure 1. Geologic map of the large-scale, low-temperature epithermal metallogenic domain in southwestern China, showing the locations of Carlin-like gold, antimony, and tin-polymetallic deposits in the Youjiang basin [7].

Carbonate minerals such as calcite and dolomite are the products of carbonatization recrystallization in Carlin-like (-type) gold deposits, and they are closely related to gold mineralization in these deposits [6,7,29]. In the northern gold deposits of Dian-Qian-Gui, including Shuiyindong, Banqi, Bojitian, Taipingdong, and Zimudang, it has been shown that the ore-stage calcite characteristics within these deposits are enriched in MREE and HREE [7,20,32–35]. However, systematic studies about gold deposits in the southern part of Dian-Qian-Gui are scarce. In this paper we have analyzed the rare earth element (REE), C, and O isotopic characteristics of calcites from the Zhesang gold deposit to constrain the origins of the ore-forming fluids. More importantly, the trace elements contents (Fe, Mn, and Mg) of calcites were combined to examine possible guidelines for prospecting gold resources.

2. Regional Geology and Alteration Types

2.1. Regional Geological Setting

The Zhesang gold deposit is located at the junction between the Qiubei–Guangnan fold belt and the eastern end of the Wenshan–Funing fold belt [36], and it is controlled by the Guangnan–Funing Fault (Figure 1). The faults of the area can be divided into two periods; the NE-trending faults are older faults, whereas the NW- and near EW-trending faults are younger (Figure 2) [28]. The width

of the NE-trending faults zone is approximately 800 m, length is around 3000 m, and dips to the SE with an angle from 60° to 70°. The NW-trending faults generally dip to the NE with an angle of about 65° [37]. Magmatic activity is extremely intense in this region, and its intrusive rocks mainly consist of diabase and gabbro-diabase, which occur as dykes (Figures 1–3 and Figure 4a,b). The effusive rocks are generally basalts. The basic rocks can be divided into two periods, the older has zircon U-Pb age of 258 ± 5 Ma, and it is viewed as a component of the Permian Emeishan large igneous province [38]. The younger has zircon U-Pb ages between 215 ± 5 Ma and 219.9 ± 6.6 Ma, and it is suggested as the product of the Indosinian movement [27,28,39].

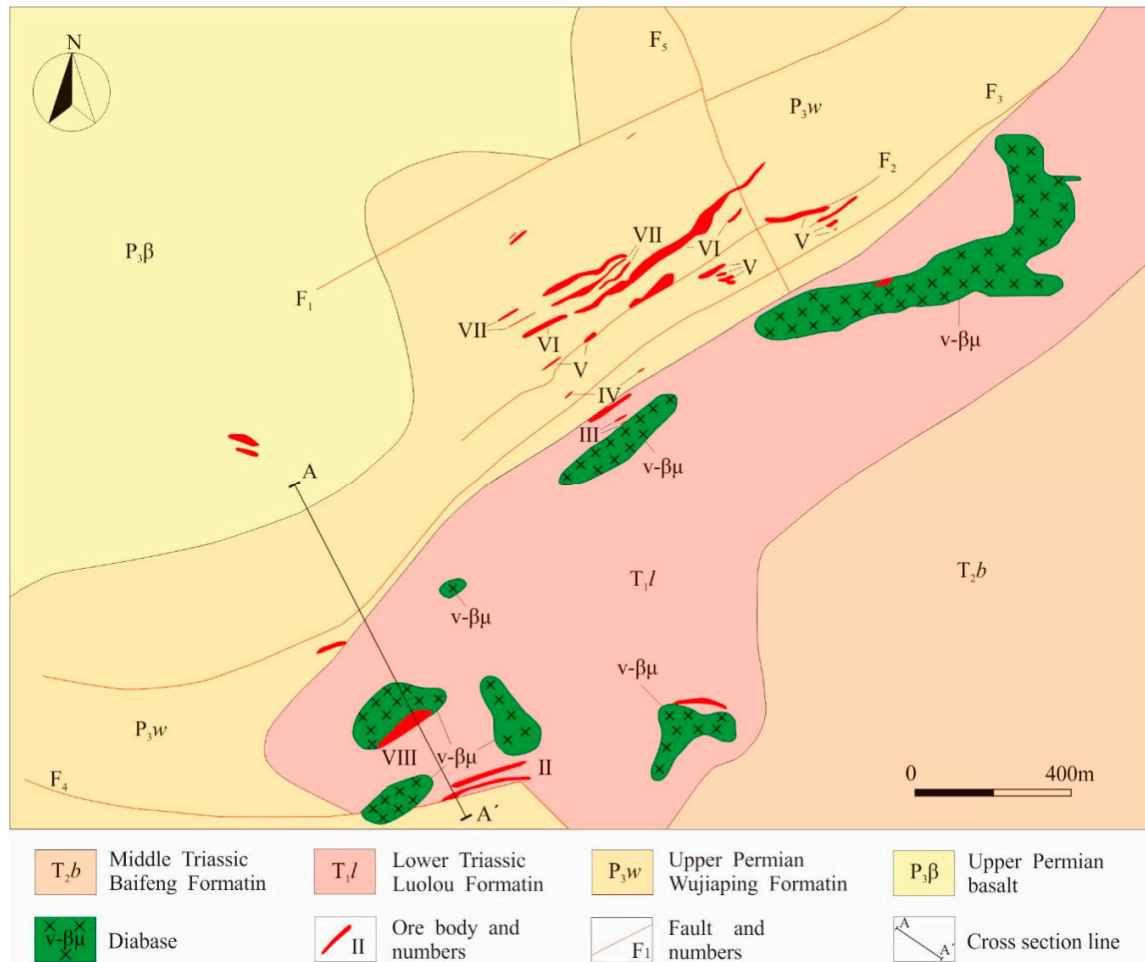


Figure 2. Geological map of the Zhesang gold deposit [39].

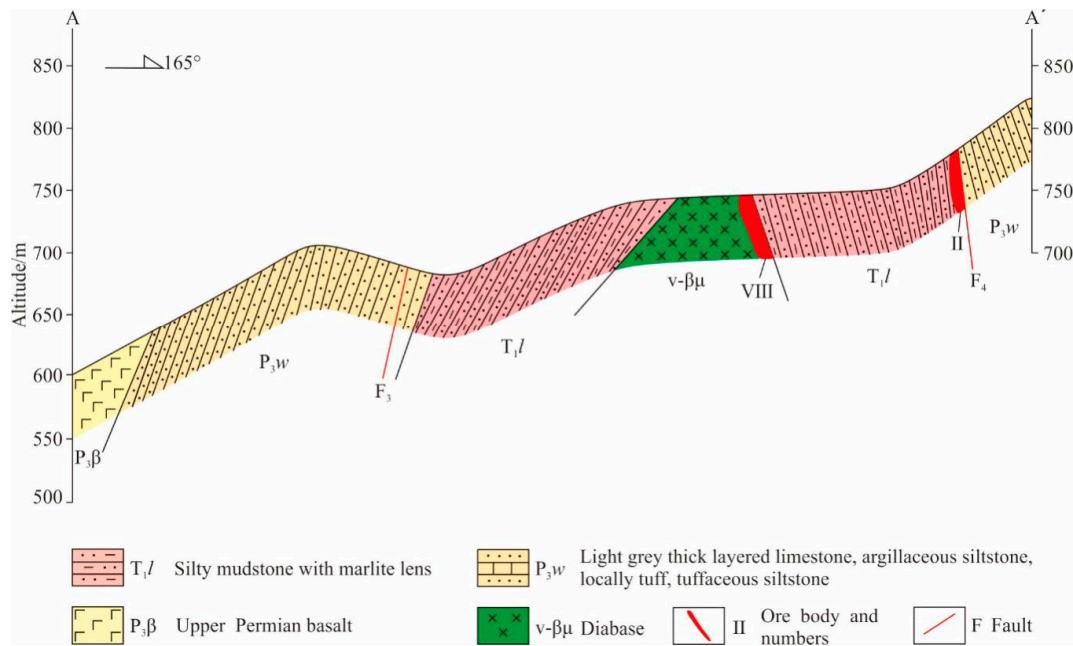


Figure 3. Regional geological cross section of the Zhesang gold deposit.



Figure 4. (a) Field photograph of diabase and its relationship with gold ore; (b) hand specimen of the diabase; (c) field photograph of ore-stage calcite with alteration halo and are crosscut by the post-ore calcite; (d) photomicrograph of the textural relationships between euhedral arsenopyrite and ore-stage calcite (reflected plane polarized light); v βμ = diabase; Sd = Sandstone; Apy = Arsenopyrite; Cc1 = Ore-stage calcites; Cc2 = Post-ore calcites.

The NEE-trending Zhesang anticlinorium, with axis trending around 60°, hinge dips to E, dip angle of around 20°, and primarily consists of the Wujiaping Formation and Luolou Formation, is the main structure of the mining area, and the gold ore bodies are mainly located at its SE limb [27–31,37]. The outcropping strata in the mining area are as follows (in increasing age): The Middle Triassic Baifeng Formation (T_{2b}), Lower Triassic Luolou Formation (T_{1l}), Upper Permian Wujiaping Formation (P_{3w}), and Upper Permian basalts ($P_{2\beta}$) (Figures 2 and 3). The outcropping orebodies in this mining area include No. I–VIII, with the largest of these orebodies being No. VI and VII. The orebodies are near-parallel trending in a NE direction. The No. I, II, V, VI, and VII orebodies are located in the organic-matter-rich carbonaceous siltstones, muddy siltstones, tuffaceous siltstones, and dolomites of the Wujiaping Formation. The No. III and VIII orebodies are located near the contact zone between the diabases and siltstones of the Lower Triassic Luolou Formation (Figures 2 and 4a). A minor amount of pyritization and arsenopyritization has been observed along the margin of gabbro-dabase dykes. The orebodies occur as 50–1000 m long stratiform lenticles, with surface outcrops that are 3–40 m wide. The density of the orebodies generally varies between 1.5 and 2.6 g/t, with a maximum of 9 g/t [40].

2.2. Alteration Features

The host-rock alteration types of the Zhesang gold deposit include pyritization, arsenopyritization, carbonatization, silicification, and argillic alteration (illite). The calcites occurring at the ore district can be divided into ore-stage and post-ore stage based on the field investigation and petrographic and mineralogical observation (Figure 4c). The ore-stage calcites occur as white or pale-yellow veins with alteration halo containing calcite, quartz, pyrite, arsenopyrite, and limonite alteration halo and are cut by the post-ore calcite. The paragenesis of calcite and gold-bearing arsenopyrite assemblages are observed in hand specimens in the ore-stage calcite veins and their alteration selvages. It is also found that the arsenopyrite exhibits a clear paragenetic relationship with the ore-stage calcites (Figure 4d), while the post-ore calcites occur as fine, white veins, and no sulfides were observed during the examination of hand specimens and microscope.

3. Sampling and Analytical Methods

Analytical tests were performed on seven ore-stage calcite samples and three post-ore calcite samples. The sampling locations and characteristics of each sample are shown in Table 1. Samples were firstly crushed into 40–60 mesh grains and then washed in ultrapure water to remove impurities. After the samples were dried, calcites were selected one by one using a binocular microscope. Finally, an agate mortar was used to ground the selected calcite samples to a fineness of 200 mesh. Analytical tests of trace elements and stable isotope were subsequently performed on these samples.

Table 1. Sampling locations and characteristics of calcite samples from the Zhesang gold deposit.

| Sample No. | Sampling Position | Occurrence | Color | Stage | Sources |
|------------|-------------------|------------|--------------|------------|-----------|
| ZS1-2 | No. II orebody | Vein | White | Ore-stage | This text |
| ZS2-2 | No. VI orebody | Vein | White | | |
| ZS2-3 | No. VI orebody | Vein | White | | |
| ZS2-4 | No. VI orebody | Vein | Light yellow | | |
| ZS2-5 | No. VI orebody | Vein | Light yellow | | |
| ZS2-6 | No. VI orebody | Vein | White | | |
| ZS2-7 | No. VI orebody | Vein | Light yellow | | |
| ZS1-1 | No. II orebody | Fine vein | White | Post-ore | |
| ZS1-3 | No. II orebody | Fine vein | White | | |
| ZS1-4 | No. II orebody | Fine vein | White | | |
| ZS VI-35 | No. V orebody | - | - | Wall rocks | [31] |
| ZS VI-36 | No. V orebody | - | - | | |

Note: ZS = Zhesang.

3.1. Trace Elements Analyses

The calcite REEs, Fe, Mn, and Mg concentrations of the studied samples were analyzed at the Institute of Geochemistry Chinese Academy of Science, using inductively coupled plasma-mass spectrometry (ICP-MS) and Inductively Coupled Plasma Optical Emission Spectrometer (ICP-OES) instrument. About 50 mg sample powder was digested with HF and HNO₃ in PTFE-lined stainless-steel bombs at 185 °C for 24 h, evaporated to dryness, and re-dissolved by 6 mL of 40% (v/v) HNO₃ at 140 °C for 3 h. The solution was introduced to ICP-MS for the measurement of REEs, and ICP-OES for Fe, Mn, and Mg analysis, and the analysis errors were ±5% and ±10%, respectively [41].

3.2. Stable Isotope Analyses

The calcite C and O isotopes of the samples were studied at the Kunming University of Science and Technology. Phosphoric acid (100%) method was used in the analytical tests. Around 60 °C, the sample reacts with phosphoric acid to release CO₂, and the C and O isotopes were determined by stable isotope mass spectrometer (Isoprime 100). Samples were placed in the Multiflow gas preparation system infused with 4 mL 100% H₃PO₄ and then vacuumed for 7–8 h for keeping the pressure at 4.0 Pa. CO₂ was separated by liquid helium, and the purified CO₂ gas was introduced to the mass spectrometer for the measurement of isotopic ratios. C and O isotope values are reported in per mil relative to V-PDB (Vienna-Pee Dee Belemnite) and V-SMOW (Vienna-Standard Mean Oceanic Water), respectively [42]. The analytical precision was ± 0.2‰.

4. Analytical Results

4.1. Rare Earth Element Characteristics of the Calcites and Wall Rocks

The REE and Y contents and chondrite-normalized patterns of the ore-stage, post-ore calcites, and wall rocks of the Zhesang gold deposit are shown in Table 2 and Figure 5. There are two widely used schemes for REE classification (excluding Y and Sc). In the first scheme, REEs are divided into light rare earth elements (LREE = La–Nd), middle rare earth elements (MREE = Sm–Ho), and heavy rare earth elements (HREE = Er–Lu); in the second scheme, REEs are divided into LREE* (LREE* = La–Eu) and HREE* (HREE* = Gd–Lu). In this work, the first scheme in combination with the chondrite-normalized REE diagrams has been used [43].

Table 2. REE data (µg/g) of calcites and wall rocks from the Zhesang gold deposit.

| Sample No. | ZS1-2 | ZS2-2 | ZS2-3 | ZS2-4 | ZS2-5 | ZS2-6 | ZS2-7 | ZS1-1 | ZS1-3 | ZS1-4 | ZS VI -35 | ZS VI -36 |
|------------|-----------|-------|-------|-------|-------|-------|----------|-------|-------|-------------------------------------|-----------|-----------|
| Stage | Ore-stage | | | | | | Post-ore | | | Wall rocks (Argillaceous Siltstone) | | |
| La | 0.48 | 0.65 | 0.54 | 1.05 | 0.76 | 0.35 | 0.89 | 1.60 | 2.86 | 1.63 | 47.20 | 55.00 |
| Ce | 1.51 | 1.71 | 1.73 | 3.97 | 2.20 | 1.23 | 2.68 | 3.95 | 6.26 | 4.16 | 90.10 | 119.00 |
| Pr | 0.25 | 0.29 | 0.26 | 0.60 | 0.30 | 0.19 | 0.33 | 0.46 | 0.61 | 0.44 | 11.70 | 16.30 |
| Nd | 1.49 | 1.65 | 1.46 | 3.46 | 1.66 | 1.15 | 1.77 | 2.20 | 2.51 | 1.90 | 47.30 | 66.70 |
| Sm | 0.80 | 0.79 | 0.75 | 1.84 | 0.89 | 0.53 | 0.80 | 0.87 | 0.73 | 0.61 | 9.14 | 11.90 |
| Eu | 0.39 | 0.34 | 0.35 | 0.77 | 0.47 | 0.22 | 0.38 | 0.76 | 1.29 | 0.81 | 2.41 | 2.77 |
| Gd | 2.34 | 1.91 | 2.03 | 4.73 | 3.03 | 1.33 | 2.39 | 1.65 | 1.00 | 0.88 | 6.57 | 8.90 |
| Tb | 0.37 | 0.30 | 0.32 | 0.70 | 0.45 | 0.21 | 0.38 | 0.27 | 0.15 | 0.14 | 0.99 | 1.55 |
| Dy | 1.85 | 1.61 | 1.64 | 3.52 | 2.31 | 1.14 | 2.02 | 1.91 | 0.97 | 0.93 | 5.59 | 8.74 |
| Ho | 0.25 | 0.24 | 0.23 | 0.51 | 0.32 | 0.18 | 0.30 | 0.39 | 0.18 | 0.18 | 0.99 | 1.69 |
| Er | 0.44 | 0.45 | 0.40 | 0.99 | 0.56 | 0.35 | 0.55 | 0.94 | 0.42 | 0.43 | 3.02 | 4.96 |
| Tm | 0.04 | 0.05 | 0.04 | 0.11 | 0.06 | 0.04 | 0.05 | 0.12 | 0.05 | 0.06 | 0.48 | 0.73 |
| Yb | 0.22 | 0.26 | 0.21 | 0.67 | 0.28 | 0.18 | 0.27 | 0.72 | 0.31 | 0.31 | 2.90 | 4.60 |
| Lu | 0.03 | 0.03 | 0.03 | 0.09 | 0.04 | 0.02 | 0.03 | 0.09 | 0.04 | 0.04 | 0.43 | 0.69 |
| Y | 12.10 | 11.60 | 11.10 | 16.40 | 12.40 | 8.56 | 11.90 | 16.40 | 7.72 | 8.02 | - | - |

Table 2. Cont.

| Sample No. | ZS1-2 | ZS2-2 | ZS2-3 | ZS2-4 | ZS2-5 | ZS2-6 | ZS2-7 | ZS1-1 | ZS1-3 | ZS1-4 | ZS VI -35 | ZS VI -36 |
|------------|-----------|-------|-------|-------|-------|-------|-------|-------|-------|-------|-----------|-----------|
| ΣREE | 10.45 | 10.27 | 9.97 | 23.01 | 13.33 | 7.13 | 12.84 | 15.91 | 17.39 | 12.51 | 228.82 | 303.53 |
| LREE | 3.73 | 4.30 | 3.99 | 9.08 | 4.92 | 2.92 | 5.67 | 8.21 | 12.24 | 8.13 | 196.3 | 257.00 |
| HREE | 0.73 | 0.79 | 0.68 | 1.86 | 0.94 | 0.59 | 0.90 | 1.87 | 0.82 | 0.84 | 6.82 | 10.98 |
| MREE | 6.00 | 5.19 | 5.32 | 12.07 | 7.47 | 3.61 | 6.27 | 5.85 | 4.32 | 3.55 | 25.69 | 35.55 |
| LREE/HREE | 5.11 | 5.44 | 5.87 | 4.88 | 5.23 | 4.95 | 6.30 | 4.39 | 14.93 | 9.68 | 28.77 | 23.41 |
| MREE/LREE | 1.61 | 1.21 | 1.33 | 1.33 | 1.52 | 1.24 | 1.11 | 0.71 | 0.35 | 0.44 | 0.13 | 0.14 |
| MREE/HREE | 8.22 | 6.57 | 7.82 | 6.49 | 7.95 | 6.12 | 6.97 | 3.13 | 5.27 | 4.23 | 3.77 | 3.24 |
| Eu/Eu* | 0.80 | 0.81 | 0.82 | 0.75 | 0.79 | 0.75 | 0.78 | 1.90 | 4.61 | 3.36 | 0.91 | 0.79 |
| Ce/Ce* | 1.02 | 0.92 | 1.09 | 1.15 | 1.08 | 1.09 | 1.15 | 1.07 | 1.07 | 1.14 | 0.88 | 0.93 |
| Sources | This text | | | | | | | | | | [31] | |

Note: $Eu/Eu^* = Eu_N/(Sm_N + Gd_N)^{0.5}$; $Ce/Ce^* = Ce_N/(La_N + Pr_N)^{0.5}$; Eu_N , Sm_N , Gd_N , Ce_N , La_N and Pr_N are normalized values using the chondritic composition of Taylor and McLennan (1985) [43].

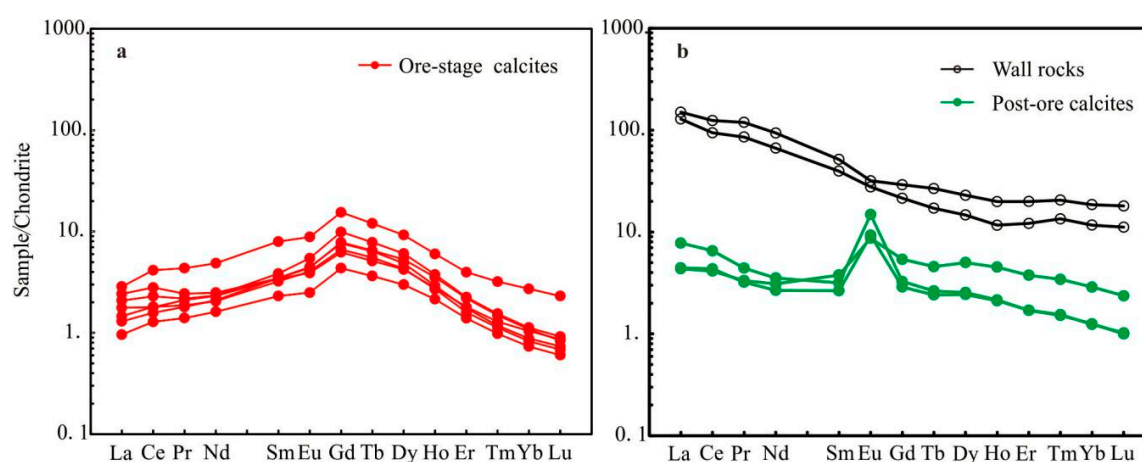


Figure 5. Chondrite-normalized REE patterns of wall rocks and calcites from the Zhesang gold deposit. (a) Ore-stage calcites; (b) Wall rocks and post-ore calcites.

(1) The ore-stage calcites have Σ REE (not including Y, and the same application below) values between 7.13 and 23.01 $\mu\text{g/g}$, and they have an REE pattern typical of MREE enrichment (MREE/LREE = 1.11–1.61, MREE/HREE = 6.12–8.22). The ore-stage calcites have a weak negative Eu anomaly ($Eu/Eu^* = 0.75$ –0.82) and no significant Ce anomaly ($Ce/Ce^* = 0.92$ –1.15).

(2) The post-ore calcites have Σ REE values between 12.51 and 17.39 $\mu\text{g/g}$, and they show moderate LREE enrichment (LREE/HREE = 4.39–14.93; MREE/LREE = 0.35–0.71), a significant positive Eu anomaly ($Eu/Eu^* = 1.90$ –4.61), and no significant Ce anomaly ($Ce/Ce^* = 1.07$ –1.14).

(3) The wall rocks (argillaceous siltstone) have high Σ REE values between 228.82 and 303.53 $\mu\text{g/g}$, and they exhibit a significant degree of LREE enrichment (LREE/HREE = 23.41–28.77; MREE/LREE = 0.13–0.14) and weak, negative Eu and Ce anomaly ($Eu/Eu^* = 0.79$ –0.91; $Ce/Ce^* = 0.88$ –0.93).

4.2. C-O Isotopic Characteristics of the Calcites

The C-O isotopic characteristics of ore-stage and post-ore calcites from the Zhesang gold deposit are shown in Table 3. The $\delta^{13}\text{C}_{V\text{-PDB}}$ values of the seven ore-stage calcite samples ranged between -3.50 and -0.90 ‰ (maximum difference of 2.6‰), with an average of -1.72 ‰. The $\delta^{18}\text{O}_{V\text{-SMOW}}$ values of the ore-stage calcite samples ranged between 11.03 and 12.49‰ (maximum difference of 1.46‰), with an average of 11.93‰. Therefore, the $\delta^{13}\text{C}_{V\text{-PDB}}$ and $\delta^{18}\text{O}_{V\text{-SMOW}}$ values of the ore-stage calcite samples vary over a relatively large range. The $\delta^{13}\text{C}_{V\text{-PDB}}$ values of the three post-ore calcite samples ranged between -1.93 and -1.02 ‰ (maximum difference of 0.91‰), and their average $\delta^{13}\text{C}_{V\text{-PDB}}$ value was -1.34 ‰. The $\delta^{18}\text{O}_{V\text{-SMOW}}$ values of these samples ranged between 16.48 and 17.14‰ (maximum

difference of 0.66‰) with an average of 16.87‰. Therefore, the $\delta^{13}\text{C}_{\text{V-PDB}}$ and $\delta^{18}\text{O}_{\text{V-SMOW}}$ values of the post-ore calcite vary over a small range.

Table 3. C-O isotopic compositions of calcites from the Zhesang gold deposit (‰).

| Sample No. | Stage | $\delta^{13}\text{C}_{\text{V-PDB}}$ | $\delta^{18}\text{O}_{\text{V-SMOW}}$ |
|------------|-----------|--------------------------------------|---------------------------------------|
| ZS1-2 | Ore-stage | −1.16 | 12.26 |
| ZS2-2 | | −1.85 | 11.70 |
| ZS2-3 | | −0.95 | 12.49 |
| ZS2-4 | | −1.90 | 11.03 |
| ZS2-5 | | −1.78 | 12.22 |
| ZS2-6 | | −3.50 | 11.76 |
| ZS2-7 | | −0.90 | 12.07 |
| ZS1-1 | Post-ore | −1.06 | 16.48 |
| ZS1-3 | | −1.02 | 17.14 |
| ZS1-4 | | −1.93 | 17.00 |

Note: V-PDB = Vienna-Pee Dee Belemnite; V-SMOW = Vienna-Standard Mean Oceanic Water.

4.3. Fe, Mn, and Mg Contents of Calcites

The Fe, Mn, and Mg contents (Table 4) of the ore-stage calcites were in the range of 4690–6300, 1007–1316, and 1080–2760 $\mu\text{g/g}$, respectively. While the post-ore calcites were in the range of 2030–2730, 1162, and 900–1680 $\mu\text{g/g}$, respectively. Hence, ore-stage calcites have significantly higher Fe contents than post-ore calcites, as the Fe contents of the former are 2–3 times of the latter. The Mn and Mg contents of the two stages samples were not significantly different.

Table 4. Fe, Mn, and Mg contents ($\mu\text{g/g}$, ppm) of calcites from the Zhesang gold deposit.

| Sample No. | ZS1-2 | ZS2-2 | ZS2-3 | ZS2-4 | ZS2-5 | ZS2-6 | ZS2-7 | ZS1-1 | ZS1-3 | ZS1-4 |
|------------|-----------|-------|-------|-------|-------|-------|-------|----------|-------|-------|
| Stage | Ore-stage | | | | | | | Post-ore | | |
| Fe | 5040 | 5880 | 6300 | 4690 | 5600 | 4690 | 5320 | 2730 | 2030 | 2100 |
| Mn | 1085 | 1239 | 1316 | 1085 | 1085 | 1162 | 1007 | 1162 | 1162 | 1162 |
| Mg | 1080 | 1920 | 1500 | 2160 | 2760 | 1440 | 2160 | 1680 | 1020 | 900 |

5. Discussion

5.1. Formation of Calcite

5.1.1. Calcite Genesis

A calcite sample may belong to one of the three genetic regimes (pegmatitic, hydrothermal, and sedimentary genesis) depending on its Yb/La and Yb/Ca ratio. Accordingly, Yb/La and Yb/Ca ratios can be used to determine the genesis and evolution of a calcite sample [44–46]. The ore-stage and post-ore calcites of the Zhesang gold deposit were projected onto a Yb/La–Yb/Ca diagram, and it was observed that all the samples fell in the hydrothermal region (Figure 6). This indicates that all calcites were formed via hydrothermal activity.

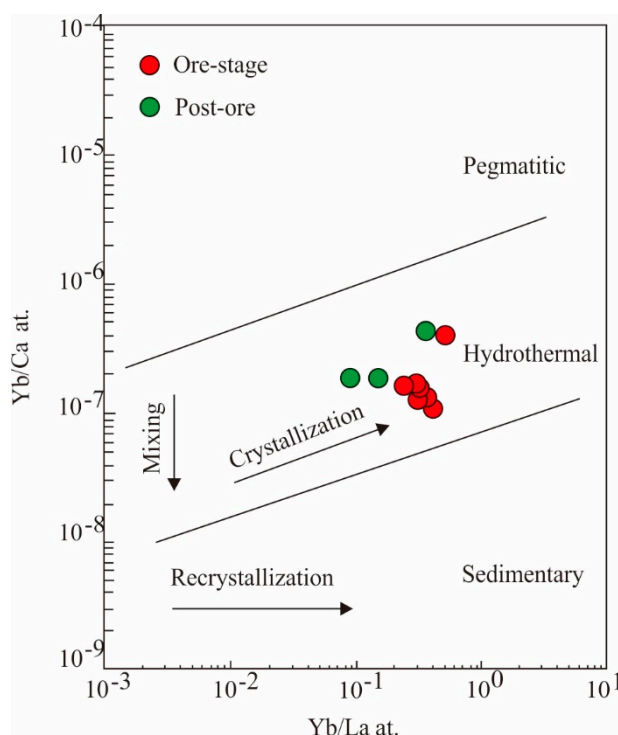


Figure 6. Yb/La vs. Yb/Ca plot for calcites from the Zhesang gold deposit [44].

As the geochemical properties of each REE are different, the cogenity of gangue minerals in a metallogenic system can be examined by comparing their LREE and HREE ratios [47–49]. Based on a study about the REE geochemistry of calcites in the Tannenboden and Beihilfe deposits, Bau and Dulski [48] observed that cogenetic gangue minerals generally exhibit a horizontal distribution in the Y/Ho–La/Ho diagram. The post-ore calcites from Zhesang show constant Y/Ho values and are horizontally distributed on the La/Ho–Y/Ho diagram, while ore-stage calcites show significantly different Y/Ho values and they do not project onto the same horizontal line (Figure 7). This may imply that post-ore calcites are cogenetic and they may have formed by a single fluid, but ore-stage calcites may be formed by a mixing of different fluids.

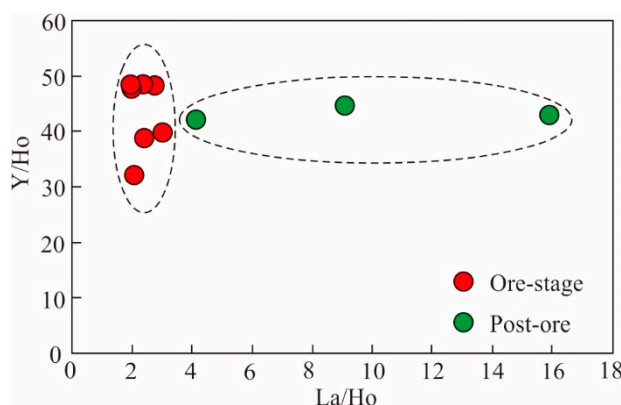


Figure 7. La/Ho vs. Y/Ho plot for calcites from the Zhesang gold deposit [48].

5.1.2. Significance of Calcite C-O Isotopic Composition

CO₂ in crustal fluids is generally derived from three source regions: (1) marine carbonate sediments with average $\delta^{13}\text{C}_{\text{V-PDB}}$ values of approximately 0‰; (2) deep sources with average $\delta^{13}\text{C}_{\text{V-PDB}}$ values of approximately –5 to –8‰; and (3) the biogenetic organic matter being isotopically light with

mean $\delta^{13}\text{C}_{\text{V-PDB}}$ values around -25‰ [50]. On the other hand, ultrabasic-basic magmatic rocks are characterized by O isotope compositions of about 5‰ [51], and the O isotopes $> 8\text{‰}$ are characteristic of supra crustal rocks like granite or rocks that have assimilated crustal materials [52]. There are five mechanisms by which CO_2 enters ore-forming fluids from these source regions: The dissolution and decarbonation of carbonate minerals, the carboxyl and oxidation of sedimentary organic matter, and the degassing that accompanies the fractional crystallization of mantle magmas [53]. As these mechanisms also lead to the co-fractionation of C and O isotopes, the mutual constraints arising from these mechanisms can be used to trace the source of CO_2 in a geological fluid [44,54,55]. The C and O isotopic data of the ore-stage and post-ore calcites were projected onto a $\delta^{18}\text{O}_{\text{V-SMOW}}-\delta^{13}\text{C}_{\text{V-PDB}}$ diagram (Figure 8). The two stages of calcites fell on the same trend of marine carbonate dissolution; however, they differ significantly in their O isotopic characteristics, and the ore-stage calcites fell on the side closer to basic rocks. As it is shown before, some orebodies of Zhesang are hosted by the diabases (Figures 2 and 4a), and the mineralization age (215.3 ± 1.9 Ma) of Zhesang is in good accordance with the forming age (219.9 ± 6.6 Ma) of basic rocks in the region [27,28]. Therefore, it is reasonable that the ore-forming fluids may be associated with the diabase outcropped in the mining district. However, there is no apparent difference in C isotope; this may have resulted from the significant differences between C and O composition in basic magma, in which O content (44.57%) is apparently higher than C content (0.14%) [54]. Li and Yao [56] showed that the average water content in basic magma is around 2.02%, and basic magma is usually poor of volatiles. This may imply that the amount of ore-forming fluids provided by the diabase is limited. Therefore, it can be concluded that the C and O isotopes of both stages of fluids were mainly sourced from meteoric water and marine carbonate interaction, but the ore-stage fluid was contaminated by a small amount of basic magmatic fluids.

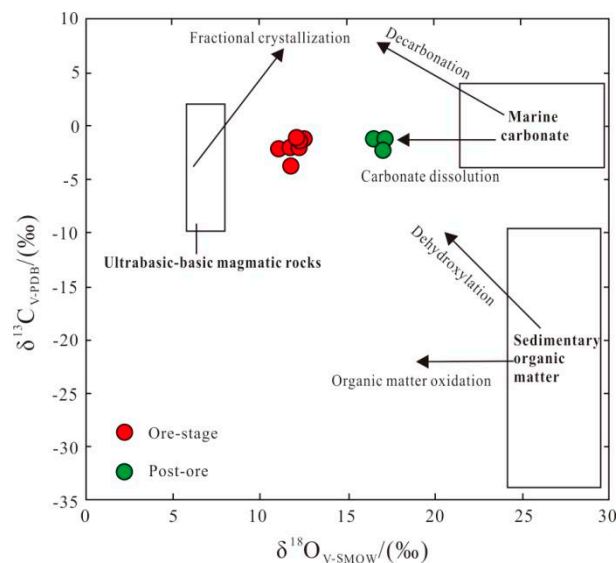


Figure 8. $\delta^{13}\text{C}_{\text{V-PDB}}$ vs. $\delta^{18}\text{O}_{\text{V-SMOW}}$ diagram of calcites from the Zhesang gold deposit [57].

The Dian-Qian-Gui Golden Triangle contains a large number of CLGDs. By reviewing the C isotopic data of calcites in the Zhesang, Shuiyindong [58], Bojitian [33], Miaolong-Paiting [59], and Taipingdong-Zimudang gold deposits [34], it was discovered that the C isotopic compositions of the calcites of the Dian-Qian-Gui region generally ranged between -8.80 and 3.51‰ V-PDB (Figure 9). Therefore, it may be concluded that the carbon in the CLGD of Dian-Qian-Gui primarily originated from marine carbonates and the deep mantle.

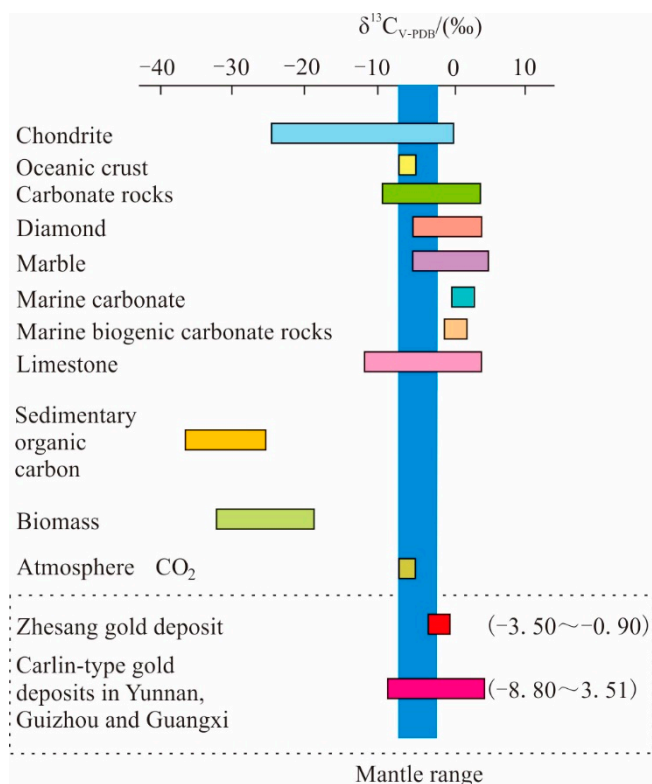


Figure 9. Comparison diagram of carbon isotopic compositions [60].

5.1.3. Significance of Calcite REE Characteristics

It is possible to discern the origin of the ore-forming materials of a deposit by comparing the REE patterns of various geological bodies to those of the hydrothermal minerals [61]. The formation of calcites is intimately accompanied with the entire mineralization process in the Zhesang gold deposit. Therefore, the REE geochemistry of the calcites can reflect the REE characteristics of the ore-forming fluids of the deposit.

The ore-stage calcites of Zhesang exhibit a typical MREE enrichment, similar to the ore-stage calcites found in many of the CLGDs in Qianxinan [22,32–34,59]. Such a characteristic is inconsistent with the significant LREE enrichment observed in post-ore calcites and the host strata (which consists of phyllitic calcareous slate, rhyolitic tuff, spilite, diabase, muddy siltstone, and tuff) [29,62]. In addition, hydrothermal fluids originated from meteoric water usually have low REE concentrations (ranging from 1 to nearly 10^{-6} times chondrite) and show an LREE-enriched pattern [61]. It is shown that REEs were not simply derived from meteoric water or host rocks. Castorina et al. [63] and Ehya [64] suggested that the REE abundance in hydrothermal fluids depends mainly on the deposition order of the REE-bearing minerals, regardless of the ultimate REE source. However, in the Zhesang ore district, or even in the whole “Dian-Qian-Gui golden triangle” region, the dominant minerals are quartz, pyrite, arsenopyrite, and calcite. It is widely accepted that these minerals, except calcite, usually have extremely low REE contents, and they do not show any tendency in combination with different types of REE (e.g., LREE, MREE or HREE). Also, there have no minor minerals typical enrichment of LREE or HREE been reported. Combined with the above discussion about C and O isotopes, and the study of the H-O isotopic characteristics (H: -70.2 – -46.5 ‰; O: 6.7 – 13.9 ‰) of fluid inclusions within quartz conducted by Gao and Huang [30], they suggested that the ore-forming fluids of the primary metallogenic stage of the deposit were derived from a mix of meteoric water and magmatic water. Hence, it is inferred that partial REE of ore-forming fluids may be sourced from basic magmatic fluids. Nonetheless, it cannot be ignored that rare earth fractionation could also have been caused by complexation, coprecipitation, adsorption, desorption, and other processes [61,65–67].

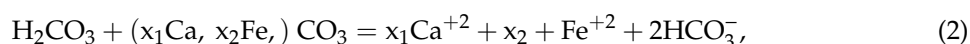
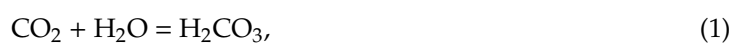
The post-ore calcites exhibit a significant degree of LREE enrichment, which is similar to the REE pattern of muddy siltstones in the host strata [31]. However, the host rocks have higher REE contents than these calcites, which also exhibit positive Eu anomalies. This indicates that the post-ore calcites were mainly formed by fluids (like meteoric water) that leached the host rocks of the mining area. The difference between the post-ore calcites and host rocks in terms of their total REE contents is indicative of the degree of REE leaching from the host rocks.

In summary, the REE, C-O isotopic data characteristics of the calcites, and H-O isotopic characteristics of fluid inclusions in quartz from the Zhesang gold deposit indicate the following: the ore-forming fluids were mainly derived from crustal fluids and a small amount of basic magmatic fluids, whereas post-ore fluids were consisted of crustal fluids generated by the infiltration of meteoric water through the host rocks.

The ore-stage calcites show weak, negative Eu anomaly, while post-ore calcites show significant, positive Eu anomaly. Generally, REE^{3+} has different properties from Ce^{4+} and Eu^{2+} . In some geochemical processes, the separation of Ce^{4+} , Eu^{2+} , and REE^{3+} will occur, and the Ce and Eu anomalies will be positive or negative [61,68–70]. Temperature is the most important parameter controlling the Eu/Eu* redox potential in a hydrothermal environment [66]. Möller et al. [71] suggested Eu anomaly is lacking or slightly positive in fluorite precipitated from a fluid with a temperature < 200 °C. At temperatures > 200 °C, Eu^{3+} is reduced to Eu^{2+} , which is very mobile and difficult to be incorporated into the fluorite structure, and therefore tends to remain in the fluid; this produces negative Eu anomalies in fluorites precipitated from a fluid with > 200 °C. The ore-stage calcites may have formed above 200 °C, which is proved by the fluid inclusion study (the homogenization temperature of ore fluids in Zhesang, 194–295 °C) conducted by Gao and Huang [30]. The high temperature may reduce Eu^{3+} to Eu^{2+} . The weak, negative Eu anomalies also indicate that the precipitation of the ore-forming fluids occurred in a weakly reducing environment. This is consistent with the large amounts of sulfides (e.g., arsenopyrites and pyrites) that appeared during the mineralization epoch. The post-ore calcite was formed under 200 °C (unpublished), and the low temperature could oxidize Eu^{2+} , which is derived from host rocks, to Eu^{3+} . Therefore, the Eu anomaly of calcites may be mainly affected by temperature [72].

5.2. Calcite Formation Process and Au Deposition

Many studies have demonstrated that gold deposition in Carlin-like (-type) gold deposits is closely related to the decarbonatization of their host strata, as this process provides the Fe required by the sulfidation processes that occurs during gold precipitation [14,20,73]. CO_2 was likely the principal acid volatile in the ore fluids and could promote dissolution of the ferroan calcite in the host rocks [1,14]:



Reaction (2) is representative of decarbonation reactions in Carlin-type systems. This reaction provides Fe elements for calcites. Fe is probably mobilized as Cl complexes in fluids, (e.g., FeCl_2). The formation of Fe-rich carbonate is due to the ion radii of Fe^{2+} being similar to Ca^{2+} , so that Fe^{2+} can easily enter the lattice of carbonate to replace Ca^{2+} . The precipitation of gold and Fe-containing sulfides (e.g., arsenopyrite and pyrite) in large quantities will also form large amounts of Fe-rich calcite simultaneously. Hence, Fe-rich carbonate is always an important product in the mineralization of Carlin-like (-type) gold deposits.

In Table 4 and Figure 10, it is shown that the Fe contents of ore-stage calcites are significantly higher than those of post-ore calcites. The different concentration of Fe^{2+} in calcite at different stages may be due to the different initial fluid Fe content. According to previous discussion about the source of ore-forming fluid, it is found that the ore-stage fluid not only comes from the crustal fluid by meteoric water leaching wall rocks, but also from the basic magmatic fluid, and the post-ore fluid

mainly comes from the dissolution of host rocks by meteoric water. These calcites are possibly formed by the following Reactions (3) and (4), respectively:

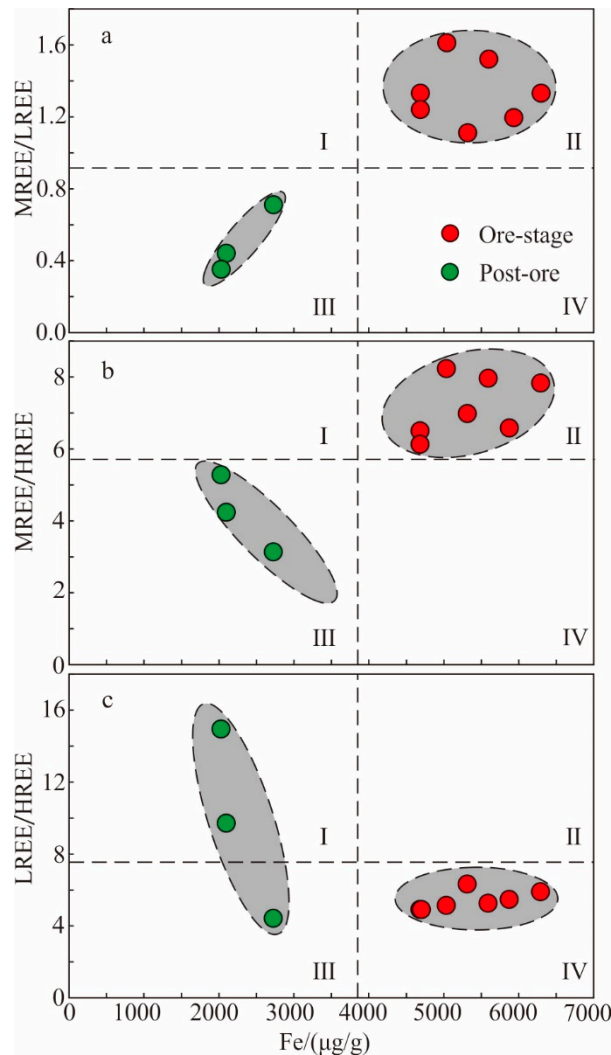
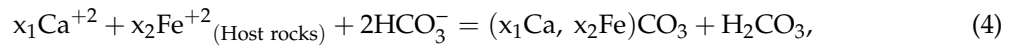
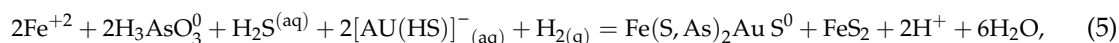


Figure 10. (a) MREE/LREE vs. Fe contents, (b) MREE/HREE vs. Fe contents plot for calcites from the Zhesang gold deposit. (a,b) I, III, IV = non-prospecting area, II = prospecting area; (c) I, II, III = non-prospecting area, IV = prospecting area.

Therefore, the ore-stage calcite Fe is not only from the dissolution of the host rocks, but also from the basic magma, while the Fe constituent of post-ore calcite mainly comes from the dissolution of host rocks.

Gold is commonly associated with sulfide minerals such as pyrite and arsenopyrite in Carlin-like (-type) gold deposits [74]. Much of this gold is present as “invisible” gold (particles less than 0.1 µm), and many studies have shown that the gold consists either of submicroscopic metallic particles or is incorporated as “chemically bound” gold [75–79]. Simon et al. [80,81] concluded that gold in arsenian pyrite occurs in solid solution (Au^{1+}) and as nanoparticles of native gold (Au^0). In ore-forming fluids, the most likely ligands for complexation with Au^+ are HS^- , Cl^- , and OH^- [82]. Deposition from gold sulfide complexes is of importance in gold precipitation processes [83]. Most models for deposition of

gold are based on the assumption that Au is transported as bisulphide complexes (e.g., $\text{Au}(\text{HS})_2^-$) [84]. Numerous studies of Carlin-type gold deposits in Nevada have concluded that gold-rich arsenian pyrite precipitated from H_2S -rich fluids, which sulfurized iron-bearing minerals in the host rocks [1,14,85]. The predominant As species was $\text{H}_3\text{AsO}_3^0_{(\text{aq})}$. Such as determined from the geochemical modeling calculations above, Zhesang gold deposit could have deposited gold-bearing arsenopyrite, possibly by the following reaction:



This reaction is strongly dependent on the activity of reduced sulfur (as H_2S or HS^-), and a decrease in H_2S produced by sulfidation would promote the formation of arsenopyrite. The reaction involves reduction of As(3+) and Au(1+) by consumption of $\text{H}_{2(\text{g})}$, which can be provided by reaction of the metal-transporting fluids with the local organic-rich sediments [16]. So Au, S, and As are migrated in the form of $[\text{Au}(\text{HS})_2]^-$, H_2S , and $\text{H}_3\text{AsO}_3^0_{(\text{aq})}$ in the ore-forming fluid. When H_2 is added to the ore-forming fluids, Au, S, and As precipitate to form invisible gold-bearing arsenopyrite and pyrite. Through the above discussion about the source of Fe constituent of calcite, it is inferred by this reaction that Au is also sourced from the host rocks and basic magmas. Such inference is also supported by the previous studies about gold contents of wall rocks and diabases and S-Pb isotopes in the Zhesang gold deposit [30,31,62]. High Au abundances have been observed in the carbonaceous and muddy siltstones of the Upper Permian Wujiaping Formation, and the fine sandstones and diabases of the Lower Triassic Luolou Formation; their Au abundances are 91.7, 6.5, and 59.5 times the Clarke value of gold (0.001 ppm) [86], respectively. Furthermore, according to the S-Pb isotopic characteristics, it is suggested that the Pb elements of the deposit mainly originated from the upper crust, with some from magmatic components [39]. Therefore, it can be concluded that the ore-forming materials of the Zhesang gold deposit include contributions both from the host strata and basic diabase rocks.

Summing up the above discussion and previous studies [27,30,31,40,87], a conceptual genetic model of the Zhesang gold deposit is proposed as follows: (1) From Late Permian to Early Triassic, large amounts of gold-bearing sandstone strata were deposited in Funing County. During Indosinian movement, the NE-striking faults and secondary fold structures were formed. Then the lithosphere began to stretch, and the NE-striking faults and secondary fold structures took place and had tensional activity, thus forming passages that enabled the flow of ore-forming fluids, as well as storage spaces for mineral deposition. (2) The intrusion of large amounts of basic magma (at about 215 Ma) [27] in this region provided some of the ore-forming materials, fluids and heat that led to gold deposition. This basic magma also heated deep-circulating waters derived from meteoric water, which leached the source strata. This led to the activation and migration of ore-forming elements (including Au) from the source strata, and ultimately induced the gold mineralization.

5.3. Guidelines Provided by Calcite REE, Fe, and O Isotopic Compositions for Gold Prospecting

All calcites found in the mining area were either ore-stage or post-ore calcites. There are significant differences between these calcites in terms of their REE patterns, Fe contents, and O isotopic compositions. Therefore, the MREE/LREE, MREE/HREE, and LREE/HREE ratios, Fe contents, and $\delta^{18}\text{O}_{\text{V-SMOW}}$ values of the calcite samples have been analyzed to examine possible guidelines that could be of use for gold prospecting (Figures 10–12).

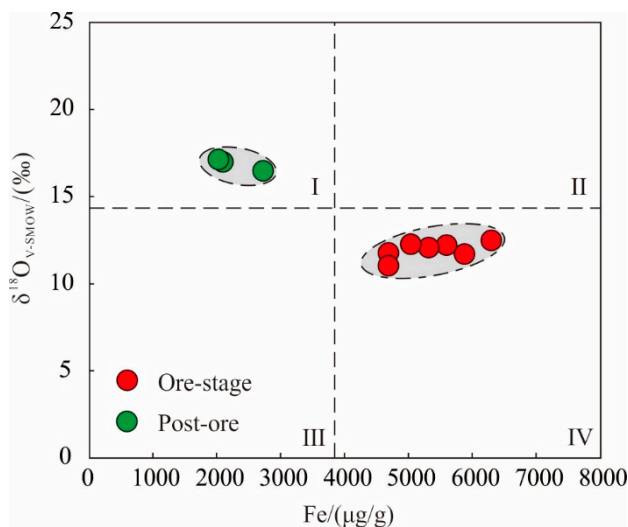


Figure 11. Fe contents vs. $\delta^{18}\text{O}_{\text{V-SMOW}}$ value plot for calcites from the Zhesang gold deposit. I, II, III = non-prospecting area; IV = prospecting area.

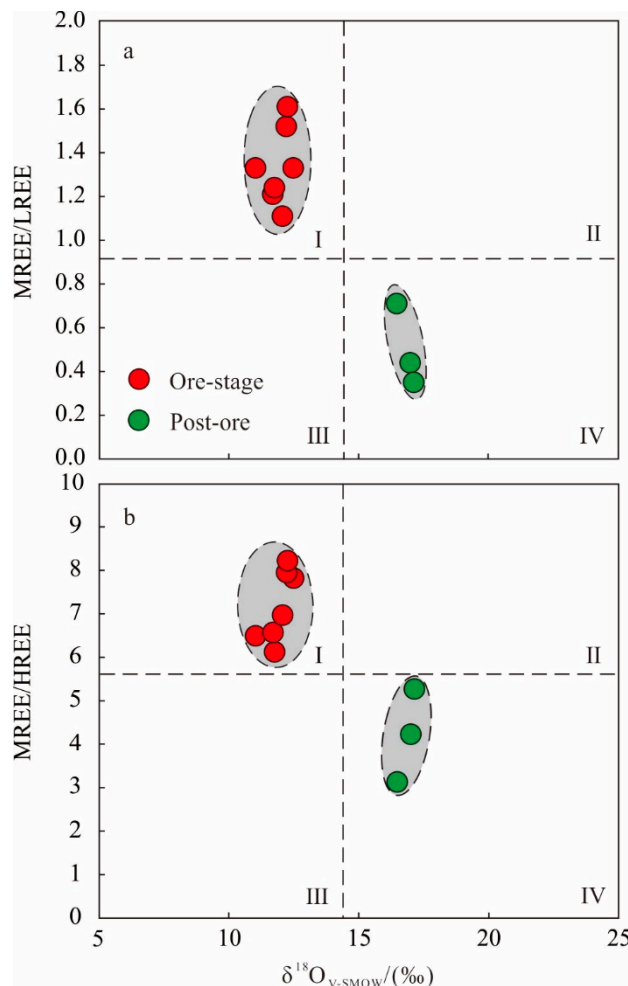


Figure 12. (a) MREE/LREE vs. $\delta^{18}\text{O}_{\text{V-SMOW}}$ value, (b) MREE/HREE vs. $\delta^{18}\text{O}_{\text{V-SMOW}}$ value plot for calcites from the Zhesang gold deposit. (a,b) I = prospecting area; II, III, IV = non-prospecting area.

The average Fe content of the seven ore-stage calcite samples (5367 $\mu\text{g/g}$) was treated as the Fe content of all ore-stage calcites; similarly, the average Fe content of the three post-ore calcite samples

(2287 $\mu\text{g/g}$) was treated as the Fe content of all post-ore calcites. The average Fe content of these calcites (3827 $\mu\text{g/g}$) was then treated as the boundary between ore-stage and post-ore calcites in terms of Fe content.

Similarly, the average MREE/LREE ratios of the ore-stage and post-ore calcite samples were treated as the MREE/LREE ratios of the ore-stage and post-ore calcites (1.34 and 0.50, respectively). The average MREE/LREE ratio (0.92) of the calcite samples was then used as the boundary between ore-stage and post-ore calcites in terms of the MREE/LREE ratio. A correlation diagram was plotted between the Fe contents and the MREE/LREE ratios of the calcite samples, which was then divided into four quadrants according to the average Fe content (3827 $\mu\text{g/g}$) and MREE/LREE ratio (0.92) of the samples (Figure 10a).

The average MREE/HREE ratios of the seven ore-stage calcite samples (7.16) and three post-ore calcite samples (4.21) were used as the representative MREE/HREE ratios of all ore-stage and post-ore calcites, respectively. The average MREE/HREE ratio of the ore-stage and post-ore calcites (5.69) was treated as the boundary between ore-stage and post-ore calcites in terms of the MREE/HREE ratio. A correlation diagram was plotted between the Fe contents and the MREE/HREE ratios of the calcite samples, which was then divided into four quadrants according to the average Fe content (3827 $\mu\text{g/g}$) and MREE/HREE ratio (5.69) of those samples (Figure 10b).

The average LREE/HREE ratios of the seven ore-stage calcite samples (5.40) and three post-ore calcite samples (9.67) were used as the representative LREE/HREE ratios of all ore-stage and post-ore calcites, respectively. The average LREE/HREE ratio between the ore-stage and post-ore calcites (7.54) was treated as the boundary that delineates ore-stage and post-ore calcites in terms of the LREE/HREE ratio. A correlation diagram was plotted between the Fe contents and the LREE/HREE ratios of the calcite samples, which was then divided into four quadrants according to the average Fe content (3827 $\mu\text{g/g}$) and LREE/HREE ratio (7.54) of the samples (Figure 10c).

The average MREE/HREE ratios of the seven ore-stage calcite samples (7.16) and three post-ore calcite samples (4.21) were used as the representative MREE/HREE ratios of all ore-stage and post-ore calcites, respectively. The average MREE/HREE ratio of the ore-stage and post-ore calcites (5.69) was treated as the boundary between ore-stage and post-ore calcites in terms of the MREE/HREE ratio. A correlation diagram was plotted between the Fe contents and the MREE/HREE ratios of the calcite samples, which was then divided into four quadrants according to the average Fe content (3827 $\mu\text{g/g}$) and MREE/HREE ratio (5.69) of these samples (Figure 10b).

The average $\delta^{18}\text{O}_{\text{V-SMOW}}$ value of the seven ore-stage calcite samples (11.93‰) and three post-ore calcite samples (16.87‰) were used as the representative $\delta^{18}\text{O}_{\text{V-SMOW}}$ value of all ore-stage and post-ore calcites, respectively. The average $\delta^{18}\text{O}_{\text{V-SMOW}}$ value of the ore-stage and post-ore calcites (14.40‰) was treated as the boundary between ore-stage and post-ore calcites in terms of the $\delta^{18}\text{O}_{\text{V-SMOW}}$ value. A correlation diagram was then plotted between the Fe contents and the $\delta^{18}\text{O}_{\text{V-SMOW}}$ values of the calcites, which was divided into four quadrants using the average Fe content (3827 $\mu\text{g/g}$) and $\delta^{18}\text{O}_{\text{V-SMOW}}$ (14.40‰) value of the calcite samples (Figure 11). Similarly, $\delta^{18}\text{O}_{\text{V-SMOW}}$ versus MREE/LREE and $\delta^{18}\text{O}_{\text{V-SMOW}}$ versus MREE/HREE correlation diagrams were plotted (Figure 10a,b), which were divided into quadrants using the average $\delta^{18}\text{O}_{\text{V-SMOW}}$ value (14.40‰), MREE/LREE value (0.92), and MREE/HREE value (5.69) of the ore-stage and post-ore calcite samples. In Figure 11c, it is shown that the LREE/HREE ratio cannot be used to distinguish the two stages calcites, which indicates that it is difficult to use the LREE/HREE ratio of a calcite sample as a prospecting guideline. Therefore, a correlation diagram was not plotted between the LREE/HREE ratios and the $\delta^{18}\text{O}_{\text{V-SMOW}}$ values of the calcite samples.

In Figure 10a,b, it is shown that all ore-stage calcites fall in the second quadrant, whereas all post-ore calcites fall in the third quadrant. In Figure 10c, all ore-stage calcites fall in the fourth quadrant, whereas all post-ore calcites fall in the first and third quadrants. In Figure 11, all ore-stage calcites fall in the fourth quadrant, whereas all post-ore calcites fall in the first quadrant. In Figure 12a,b, all ore-stage calcites fall in the first quadrant, whereas all post-ore calcites fall in the fourth quadrant.

As a whole, it is shown that the ore-stage calcites generally have Fe contents greater than 3827 $\mu\text{g/g}$, whereas the post-ore calcites lower than 3827 $\mu\text{g/g}$. In terms of REE ratios, the ore-stage calcites generally have MREE/LREE ratios greater than 0.92, whereas the post-ore calcites lower than 0.92. The MREE/HREE ratios of the ore-stage calcites and post-ore calcites are generally greater and lower than 5.69, respectively, thus indicating that the ore-stage calcites have a greater degree of MREE enrichment than the post-ore calcites. In terms of the O isotopic indicator ($\delta^{18}\text{O}_{\text{V-SMOW}}$), the ore-stage and post-ore calcites generally have $\delta^{18}\text{O}_{\text{V-SMOW}}$ values lower and greater than 14.40‰, respectively.

Therefore, the MREE/LREE ratio (0.92), MREE/HREE ratio (5.69), Fe content (3827 $\mu\text{g/g}$), and $\delta^{18}\text{O}_{\text{V-SMOW}}$ value (14.40‰) of calcites in the Zhesang gold deposit can be used as prospecting guidelines. If a calcite sample falls in the second quadrant of Figure 10a,b, the fourth quadrant of Figure 11, and the first quadrant of Figure 12a,b, it is implied that the calcite sample was present during the hydrothermal event that occurred during gold mineralization. Hence, these geochemical features could potentially serve as prospecting guidelines. The mineralization of CLGD leads to the formation of calcites enriched in MREEs and relatively depleted in LREEs and HREEs. Other than the Zhesang gold deposit, this characteristic is also widely observed in the CLGD of Qianxinan Prefecture [7,22,32–35]. Wang et al. [32] discovered that calcites in the Banqi gold deposit of Qianxinan are enriched in Fe and MREEs. Yan et al. [88] found that the C-O isotope and La/Gd ratio of calcite in the CLGD of Qianxinan could be used to construct the function model to guide the prospecting guidelines, and the accuracy was as high as 100%. Tan et al. [35] suggested that C and O isotope ratios have a significant role in mineral exploration by delineating regions of rocks that have been altered by ore-forming fluids. On the other hand, C and O isotope compositions from typical unaltered limestone to high-grade ores have been used to map the extent of hydrothermal systems and have provided useful guides for the exploration of hydrothermal deposits worldwide [89–93], particularly for Carlin-type gold deposits in Nevada, USA. O isotopes of carbonate in host rocks were measured and show marked depletion proximal to gold mineralization for Carlin-type gold deposits at Vantage [94], Carlin [95], Pipeline [96,97], Screamer [98], and Banshee [99]. Calcites are major gangue minerals in Carlin-like (-type) gold deposits, and are found in most of the CLGD of southeastern Yunnan. Therefore, the aforementioned indicators may serve as important guidelines for gold prospecting in this region.

6. Conclusions

(1) The calcites that outcrop in the mining area of the Zhesang gold deposit are either ore-stage or post-ore calcites. Although both stages of calcites were formed by hydrothermal fluids, they have different sources. Based on the REE and C-O isotopic characteristics of the calcites, it is determined that the precipitating fluids of ore-stage calcite were mainly derived from crustal fluids and a small amount of basic magmatic fluids, while the formation of post-ore calcite might be derived from fluid/rock interaction between meteoric water and marine carbonates. Hence, the diabases outcropping in the mining area may be related to gold mineralization. It is further deduced that the basic magmatic activity during the Indosinian movement provided some of the ore-forming materials and fluids and heat for gold mineralization in Zhesang.

(2) The ore-stage calcites from Zhesang gold deposit exhibit a significant enrichment of MREE, a relative enrichment of Fe, and somewhat low $\delta^{18}\text{O}_{\text{V-SMOW}}$ values. If a calcite sample exhibits a MREE/LREE ratio greater than 0.92, MREE/HREE ratio greater than 5.69, Fe content greater than 3827 $\mu\text{g/g}$, and $\delta^{18}\text{O}_{\text{V-SMOW}}$ value less than 14.40‰, it is an ore-stage calcite, and these are important prospecting guidelines.

(3) Calcites are major gangue minerals in the CLGD of the Dian-Qian-Gui region. Studies about the geochemical characteristics of calcites (including their REE, Fe, $\delta^{18}\text{O}$, etc.) could provide important tools for the prospecting of CLGD.

Author Contributions: Formal analysis, Z.H.; Investigation, J.C. and T.W.; Methodology, C.L.; Visualization, J.C. and H.H.; Writing—original draft, J.W.; Writing—review & editing, J.W. All authors have read and agreed to the published version of the manuscript.

Funding: This research was funded by the National Natural Science Foundation of China, grant number 41772070, 41303038 and Open Fund of State Key Laboratory of Ore Deposit Geochemistry, grant number 201502.

Acknowledgments: We are grateful to Fujia Jia (Faculty of Land Resource Engineering of Kunming University of Science and Technology) for C-O analyses; Jing Hu, Yan Huang, and Yifan Yin (State Key Laboratory of Ore Deposit Geochemistry, Institute of Geochemistry, CAS, China) for REE, Fe, and Mn analyses; and Changbi Yang and Zhian Ma (Bureau of Geology and Mineral Resources Exploration in Yunnan Province the Second Geological Brigade) for field work.

Conflicts of Interest: The authors declare no conflicts of interest.

References

1. Hofstra, A.H.; Leventhal, J.S.; Northrop, H.R.; Landis, G.P.; Rye, R.O.; Birak, D.J.; Dahl, A.R. Genesis of sediment-hosted disseminated-gold deposits by fluid mixing and sulfidization: Chemical-reaction-path modeling of ore-depositional processes documented in the Jerritt Canyon district, Nevada. *Geology* **1991**, *19*, 36–40. [[CrossRef](#)]
2. Cline, J.S.; Hofstra, A.H.; Muntean, J.L.; Tosdal, R.M.; Hickey, K.A. Carlin-type gold deposits in Nevada: Critical geologic characteristics and viable models. *Econ. Geol. 100th Anniv. Vol.* **2005**, *100*, 451–484.
3. Emsbo, P.; Groves, D.I.; Hofstra, A.H.; Bierlein, F.P. The giant Carlin gold province: A protracted interplay of orogenic, basinal, and hydrothermal processes above a lithospheric boundary. *Miner. Depos.* **2006**, *41*, 517–525. [[CrossRef](#)]
4. Cline, J.S.; Muntean, J.L.; Gu, X.X.; Xia, Y. A comparison of Carlin-type gold deposits: Guizhou Province, Golden Triangle, Southwest China, and Northern Nevada, USA. *Earth Sci. Front.* **2013**, *20*, 1–18.
5. Xie, Z.J.; Xia, Y.; Cline, J.S.; Yan, B.W.; Wang, Z.P.; Tan, Q.P.; Wei, D.T. Comparison of the native antimony-bearing Paiting gold deposit, Guizhou Province, China, with Carlin-type gold deposits, Nevada, USA. *Miner. Depos.* **2017**, *52*, 69–84. [[CrossRef](#)]
6. Xie, Z.J.; Xia, Y.; Cline, J.S.; Alan, K.; Wei, D.T.; Tan, Q.P.; Wang, Z.P. Are there Carlin-type Au deposits in China. A comparison between the Guizhou China and Nevada USA deposits. *Rev. Econ. Geol.* **2018**, *20*, 187–233.
7. Su, W.C.; Dong, W.D.; Zhang, X.C.; Shen, N.P.; Hu, R.Z.; Hofstra, A.H.; Cheng, L.Z.; Xia, Y.; Yang, K.Y. Carlin-type gold deposits in the Dian-Qian-Gui “Golden Triangle” of southwest China. *Rev. Econ. Geol.* **2018**, *20*, 157–185.
8. Wang, Q.F.; Groves, D. Carlin-style gold deposits, Youjiang Basin, China: Tectono-thermal and structural analogues of the Carlin-type gold deposits, Nevada, USA. *Miner. Depos.* **2018**, *53*, 909–918. [[CrossRef](#)]
9. Hu, R.Z.; Su, W.C.; Bi, X.W.; Tu, G.Z.; Hofstra, A.H. Geology and geochemistry of Carlin-type gold deposits in China. *Miner. Depos.* **2002**, *37*, 378–392.
10. Zaw, K.; Peters, S.G.; Cromie, P.; Burrett, C.; Hou, Z.Q. Nature, diversity of deposit types and metallogenic relations of South China. *Ore Geol. Rev.* **2007**, *31*, 3–47. [[CrossRef](#)]
11. Peters, S.G.; Huang, J.; Li, Z.P.; Jing, C.G. Sedimentary rock-hosted Au deposits of the Dian-Qian-Gui area, Guizhou, and Yunnan Provinces, and Guangxi district, China. *Ore Geol. Rev.* **2007**, *31*, 170–204. [[CrossRef](#)]
12. Chen, M.H.; Mao, J.W.; Li, C.; Zhang, Z.Q.; Dang, Y. Re–Os isochron ages for arsenopyrite from Carlin-like gold deposits in the Yunnan–Guizhou–Guangxi “golden triangle”, southwestern China. *Ore Geol. Rev.* **2015**, *64*, 316–327. [[CrossRef](#)]
13. Li, Z.P.; Peters, S.G. *Comparative geology and Geochemistry of Sedimentary-Rock-Hosted (Carlin Type) Gold Deposits in the People’s Republic of China and in Nevada, USA*; U. S. Geological Survey Open-File Reports; USGS: Reston, VA, USA, 1998; pp. 98–466.
14. Hofstra, A.H.; Cline, J.S. Characteristics and models for Carlin-type gold deposits. *Rev. Econ. Geol.* **2000**, *13*, 163–220.
15. Reich, M.; Kesler, S.E.; Utsunomiya, S.; Palenik, C.S.; Chryssoulis, S.L.; Ewing, R.C. Solubility of gold in arsenian pyrite. *Geoch. Cosmo Acta* **2005**, *69*, 2781–2796. [[CrossRef](#)]
16. Su, W.C.; Heinrich, C.A.; Pettke, T.; Zhang, X.C.; Hu, H.R.; Xia, B. Sediment-hosted gold deposits in Guizhou, China: Products of wall-rock sulfidation by deep crustal fluids. *Econ. Geol.* **2009**, *104*, 73–93. [[CrossRef](#)]
17. Hou, L.; Peng, H.J.; Ding, J.; Zhang, J.R.; Zhu, S.B.; Wu, S.Y.; Wu, Y.; Ouyang, H.G. Textures and in situ chemical and isotopic analyses of pyrite, Huijiabao trend, Youjiang basin, China: Implications for paragenesis and source of sulfur. *Econ. Geol.* **2016**, *111*, 331–353. [[CrossRef](#)]

18. Cline, J.S.; Hofstra, A.A. Ore-fluid evolution at the Getchell Carlin-type gold deposit, Nevada, USA. *Eur. J. Mineral.* **2000**, *12*, 195–212. [[CrossRef](#)]
19. Arehart, G.B. Characteristics and origin of sediment-hosted disseminated gold deposits: A review. *Ore Geol. Rev.* **1996**, *16*, 383–403. [[CrossRef](#)]
20. Emsbo, P.; Hofstra, A.H. Rigin and significance of postore dissolution collapse breccias cemented with calcite and barite at the Meikel gold deposit, Northern Carlin trend, Nevada. *Econ. Geol.* **2003**, *98*, 1243–1252. [[CrossRef](#)]
21. Muntean, J.L.; Cline, J.S.; Simon, A.C.; Longo, A.A. Magmatic-hydrothermal origin of Nevada's Carlin-type gold deposits. *Nat. Geosci.* **2011**, *4*, 122–127. [[CrossRef](#)]
22. Su, W.C.; Hu, R.Z.; Xia, B.; Xia, Y.; Liu, Y.P. Calcite Sm-Nd isochron age of the Shuiyindong Carlin-type gold deposit, Guizhou, China. *Chem. Geol.* **2009**, *258*, 269–274. [[CrossRef](#)]
23. Hofstra, A.H.; Zhang, X.C.; Emsbo, P.; Hu, R.Z.; Su, W.C.; Christiansen, W.D.; Fu, S.W.; Theodorakos, P. Source of ore fluids in Carlin-type gold deposits in the Dian-Qian-Gui area and West Qinling belt, P.R. China: Implications for genetic models. In *Mineral Deposits Research: Meeting the Global Challenge*; Mao, J.W., Bierlein, F.P., Eds.; Springer-Verlag: Heidelberg, Germany, 2005; Volume 1, pp. 533–536.
24. Peng, Y.W.; Gu, X.X.; Zhang, Y.M.; Liu, L.; Wu, C.Y.; Chen, S.Y. Ore-forming process of the Huijiabao gold district, southwestern Guizhou Province, China: Evidence from fluid inclusions and stable isotopes. *J. Asian Earth Sci.* **2014**, *93*, 89–101. [[CrossRef](#)]
25. Jia, D.C.; Hu, R.Z. Analysis of genesis of Carlin-type gold deposits in Yunnan-Guizhou-Guangxi triangle area. *Miner Depos.* **2001**, *20*, 378–384 (In Chinese with English abstract).
26. Zhou, Y.G.; Liu, J.S.; Wang, Z.H.; Ouyang, Y.F.; Gao, Q.Z.; Liu, D.L.; Huang, Y.Y. The sources of ore-forming substance of Carlin-type gold deposit: A discussion based on the characteristics of regional stratigraphic geochemical evolution in “Gold-Triangle” area of Yunnan, Guizhou, Guangxi Provinces. *Earth Sci. Front.* **2009**, *16*, 199–208 (In Chinese with English abstract).
27. Pi, Q.H.; Hu, R.Z.; Peng, K.Q.; Wu, J.B.; Wei, Z.W.; Huang, Y. Geochronology of the Zhesang gold deposit and mafic rock in Funing County of Yunnan Province, with special reference to the dynamic background of Carlin-type gold deposits in the Dian-Qian-Gui region. *Acta Petrol. Sin.* **2016**, *32*, 3331–3342 (In Chinese with English abstract).
28. Wei, C.W.; Pi, Q.H.; Hu, R.Z.; Hu, Y.H.; Wu, J.B.; Li, G.; Yang, X. Geochemical characteristics of two stages of basic dykes and gold mineralization at Funing, Yunnan Province, China. *Acta Mineral. Sin.* **2018**, *39*, 449–514 (In Chinese with English abstract).
29. Zhang, J.Q. Ore characteristics and modes of occurrence of gold in the Zhesang gold deposit, Yunnan. *Geol. Miner. Res. South China* **2014**, *30*, 383–388 (In Chinese with English abstract).
30. Gao, Y.P.; Hang, C.J. Characteristics of the ore-forming fluid of the Zhesang Carlin-type gold deposit, Yunnan Province and their implications to the gold mineralization. *Bull. Mineral. Petrol. Geochem.* **2018**, *37*, 1062–1073 (In Chinese with English abstract).
31. Dai, H.Z.; Chen, C.H.; Liu, J.J.; Zhang, Y.; He, C.X. Elemental geochemical characteristics of the Zhesang gold deposit in the Yunnan Province and their geological significance. *Bull. Mineral. Petrol. Geochem.* **2015**, *34*, 744–754 (In Chinese with English abstract).
32. Wang, J.S.; Han, Z.C.; Li, C.; Gao, Z.H.; Yang, Y.; Zhou, G.C. REE, Fe and Mn contents of calcites and their prospecting significance for the Banqi Carlin-type gold deposit in southwestern China. *Geotecton. Metallog.* **2018**, *42*, 494–504 (In Chinese with English abstract).
33. Zhang, Y.; Xia, Y.; Wang, Z.P.; Yan, B.W.; Fu, Z.K.; Chen, M. REE and stable isotope geochemical characteristics of Bojitian gold deposit, Guizhou Province. *Earth Sci. Front.* **2010**, *17*, 385–395 (In Chinese with English abstract).
34. Wang, Z.P.; Xia, Y.; Song, X.Y.; You, B.; Zheng, X.H.; Wang, X.Y. Isotopes and REE characteristic and ore-forming materials source of the Taipingdong-Zimudang gold deposit. *Acta Mineral. Sin.* **2012**, *32*, 93–100 (In Chinese with English abstract).
35. Tan, Q.P.; Xia, Y.; Wang, X.Q.; Xie, Z.J.; Wei, D.T. Carbon-oxygen isotopes and rare earth elements as an exploration vector for Carlin-type gold deposits: A case study of the Shuiyindong gold deposit, Guizhou Province, SW China. *J. Asian Earth Sci.* **2017**, *148*, 1–12. [[CrossRef](#)]
36. Wu, Z.Q.; Wang, W.G.; He, Y.L. Funing micrograined disseminated Au deposit and its perspective. *Yunnan Geol.* **2007**, *26*, 49–55 (In Chinese with English abstract).

37. Pan, G.S.; Hu, G.M.; Xiang, Q.; Lin, F. Analysis on ore controlling condition and prospecting direction of Zhesang gold deposit in Funing of Yunnan. *Guizhou Geol.* **2014**, *3*, 190–194 (In Chinese with English abstract).
38. Jiang, W.; Xiang, Z.J.; Xia, W.J.; Xia, L.; Zhang, H.; Pham, V.T.; Yan, Q.R.; Wei, W. Are the mafic intrusive rocks in the Funing area, Southeast Yunnan (Southwest China), really derived from the Emeishan plume? New evidence from geological surveys of the Dongbo and Guichao sheets (1:50000). *Acta Petrol. Sin.* **2017**, *33*, 3109–3122 (In Chinese with English abstract).
39. Pi, Q.H.; Hu, R.Z.; Xiong, B.; Li, Q.L.; Zhong, R.C. In situ SIMS U-Pb dating of hydrothermal rutile: Reliable age for the Zhesang Carlin-type gold deposit in the golden triangle region, SW China. *Miner. Depos.* **2017**, *52*, 1179–1190. [[CrossRef](#)]
40. Zhang, Y.M.; Gu, X.X.; Bai, X.; Liu, R.P.; Zheng, L.; Wu, C.Y.; Peng, Y.W. Sulfur and lead isotopic composition characteristics of the Zhesang gold deposit in Funing county, Yunnan. *Earth Sci. Fron.* **2013**, *20*, 032–039 (In Chinese with English abstract).
41. Qi, L.; Hu, J.; Grégoire, D.C. Determination of trace elements in twenty-six Chinese geochemistry reference materials by inductively coupled plasma mass spectrometry. *Geostand. Newsl. J. Geostand. Geoanal.* **2000**, *24*, 51–63.
42. Hechmi, G.; Boni, M.; Giuliana, B.; Giuseppe, A.; Nicola, M.; Michael, J.; Salah, B.; Bouhleb, S.; Balassone, G. C–O stable isotopes geochemistry of Tunisian nonsulfide zinc deposits: A first look. *Minerals* **2018**, *8*, 13. [[CrossRef](#)]
43. Taylor, S.R.; McLennan, S.M. *The Continental Crust: Its Composition and Evolution*; Blackwell Scientific: Boston, MA, USA, 1985; pp. 1–328.
44. Möller, P.; Parekh, P.P.; Schneider, H.J. The application of Tb/Ca-Tb/La abundance ratios to problems of fluorite genesis. *Miner. Depos.* **1976**, *11*, 111–116. [[CrossRef](#)]
45. Subías, I.; Fernández-Nieto, C. Hydrothermal events in the Valle De Tena (Spanish Western Pyrenees) as evidenced by fluid inclusions and trace-element distribution from fluorite deposits. *Chem. Geol.* **1995**, *124*, 267–282. [[CrossRef](#)]
46. Shuang, Y.; Niu, H.C.; Zhao, J.X.; Bao, Z.W.; Sun, W.D. Ore-fluid geochemistry and metallogeny of the Dundee iron-zinc deposit in western Tianshan, Xinjiang, China: Evidence from fluid inclusions, REE and C-O-Sr isotopes of calcite. *Ore Geol. Rev.* **2018**, *100*, 441–456.
47. Lottermoser, B.G. Rare earth elements and hydrothermal ore formation processes. *Ore Geol. Rev.* **1992**, *7*, 25–41. [[CrossRef](#)]
48. Bau, M.; Dulski, P. Comparative study of yttrium and rare-earth behaviors in fluorine-rich hydrothermal fluids. *Contrib. Mineral. Petrol.* **1995**, *119*, 213–223. [[CrossRef](#)]
49. Huang, Z.L.; Li, X.B.; Zhou, M.F.; Li, W.B.; Jin, Z.G. REE and C-O isotopic geochemistry of calcites from the world-class Huize Pb-Zn deposits, Yunnan, China: Implications for the ore genesis. *Acta Geol. Sin.* **2010**, *84*, 597–613. [[CrossRef](#)]
50. Hoefs, J. *Stable Isotope Geochemistry*, 6th ed.; Springer-Verlag: Berlin, Germany, 2009.
51. Keyser, G.M.; Mader, D.L. O'Neill, J.A. Method for Isotope Replenishment in an Exchange Liquid Used in a Laser Induced Isotope Enrichment Process. U.S. Patent No 4,620,909, 11 April 1986.
52. Taylor, B.E. Magmatic volatiles: Isotope variation of C, H, and S. *Rev. Mineral.* **1986**, *16*, 185–662.
53. Johnson, J.W.; Oelkers, E.H.; Helgeson, H.C. SUPCRT92: A software package for calculating the standard molal thermodynamic properties of minerals, gases, aqueous species, and reactions from 1 to 5000 bar and 0 to 1000 °C. *Comput. Geosci.* **1992**, *18*, 899–947. [[CrossRef](#)]
54. Hoefs, J. *Stable Isotope Geochemistry*, 4th ed.; Springer: Berlin, Germany, 1997; pp. 65–168.
55. Liu, J.M.; Liu, J.J. Basin fluid genetic model of sediment-hosted microdisseminated gold deposits in the gold-triangle area between Guizhou, Guangxi and Yunnan. *Acta Mineral. Sin.* **1997**, *17*, 456–498 (In Chinese with English abstract).
56. Li, T.; Yao, J.L. The average chemical composition of igneous rocks in China. *Acta Geol. Sin.* **1963**, *43*, 271–280 (In Chinese with English abstract).
57. Guo, L.N.; Hou, L.; Liu, S.S.; Nie, F. Rare earth elements geochemistry and C-O isotope characteristics of hydrothermal calcites: Implications for fluid-rock reaction and ore-forming processes in the Phapon gold deposit, NW Laos. *Minerals* **2018**, *8*, 438. [[CrossRef](#)]

58. Zhou, M.F.; Zhao, J.H.; Qi, L.; Su, W.C.; Hu, R.Z. Zircon U-Pb geochronology and elemental and Sr-Nd isotope geochemistry of Permian mafic rocks in the Funing area, SW China. *Contrib. Mineral. Petrol.* **2006**, *151*, 1–19. [[CrossRef](#)]
59. Guo, J.H.; Chen, S.W.; Gui, X.D. Geological characteristics of Jinba gold deposit in southeast Yunnan. *J. Precious Met. Geol.* **2001**, *10*, 71–79 (In Chinese with English abstract).
60. Mao, J.W.; Wang, Z.L.; Li, H.M.; Wang, C.Y.; Chen, Y.C. Carbon and oxygen isotope components in the Permian Basalt-hosted Copper Deposit in Ludian Area, Yuanan: Implication for the mineralization process. *Geo. Rev.* **2003**, *49*, 610–615 (In Chinese with English abstract).
61. Bau, M. Rare-earth element mobility during hydrothermal and metamorphic fluid-rock interaction and the significance of the oxidation state of europium. *Chem. Geol.* **1991**, *93*, 219–230. [[CrossRef](#)]
62. Dai, H.Z. Genetic Mineralogy of the Zhesang Glod Deposit in Funing, Yunnan Province. Master's Thesis, Chengdu University of Technology, Chengdu, China, 2012. (In Chinese with English abstract).
63. Castorina, F.; Masi, U.; Padalino, G.; Palomba, M. Trace-element and Sr-Nd isotopic evidence for the origin of the Sardinian fluorite mineralization (Italy). *Appl. Geochem.* **2008**, *23*, 2906–2921. [[CrossRef](#)]
64. Ehya, F. Variation of mineralizing fluids and fractionation of REE during the emplacement of the vein-type fluorite deposit at Bozijan, Markazi Province, Iran. *J. Geochem. Explor.* **2012**, *112*, 93–106. [[CrossRef](#)]
65. Chesley, J.T.; Halliday, A.N.; Scrivener, R.C. Samarium-Neodymium direct dating of fluorite mineralization. *Science* **1991**, *252*, 949–951. [[CrossRef](#)]
66. Bau, M.; Möller, P. Rare earth element fractionation in metamorphogenic hydrothermal calcite, magnesite and siderite. *Mineral. Petrol.* **1992**, *45*, 231–246. [[CrossRef](#)]
67. Michard, A. Rare earth element systematics in hydrothermal fluids. *Geochim. Cosmochim. Acta* **1989**, *53*, 745–750. [[CrossRef](#)]
68. Fulignati, P.; Gioncada, A.; Sbrana, A. Rare-earth element (REE) behaviour in the alteration facies of the active magmatic hydrothermal system of Vulcano (Aeolian Islands, Italy). *J. Volcanol. Geotherm. Res.* **1999**, *88*, 325–342. [[CrossRef](#)]
69. Chen, Y.J.; Fu, S.G. Variation of REE patterns in early Precambrian sediments: Theoretical study and evidence from the southern margin of the northern China craton. *Chin. Sci. Bull.* **1991**, *13*, 1100–1104.
70. Chen, Y.J.; Zhao, Y.C. Geochemical characteristics and evolution of REE in the Early Precambrian sediments: Evidences from the southern margin of the North China craton. *Episodes* **1997**, *20*, 109–116.
71. Möller, P.; Bau, M.; Dulski, P.; Lüders, V. REE and Y fractionation in fluorite and their bearing on fluorite formation. In *Proceedings of the 9th Quadrennial IAGOD Symp*; Schweizerbart: Stuttgart, Germany, 1998; pp. 575–592.
72. Schwinn, G.; Markl, G. REE systematics in hydrothermal fluorite. *Chem. Geol.* **2005**, *216*, 225–248. [[CrossRef](#)]
73. Su, W.C.; Xia, B.; Zhang, H.T.; Zhang, X.C.; Hu, R.Z. Visible gold in arsenian pyrite at the Shuiyindong Carlin-type gold deposit, Guizhou, China: Implications for the environment and processes of ore formation. *Ore Geol. Rev.* **2008**, *33*, 667–679. [[CrossRef](#)]
74. Boyle, R.W. *Gold: History and Genesis of Deposits*; Van Nostrand-Reinhold Company: New York, NY, USA, 1987; pp. 583–585.
75. Cabri, L.J. The distribution of trace precious metals in minerals and mineral products. *Min. Mag.* **1992**, *56*, 289–308. [[CrossRef](#)]
76. Cathelineau, M.; Boiron, M.C.; Holliger, P.; Marion, P.; Denis, M. Gold in arsenopyrite: Crystal chemistry, location and state, physical and chemical conditions of deposition. In *The Geology of Gold Deposits: The Perspective in 1988*; Economic Geology Monograph 6; Keays, R.R., Ramsay, R., Groves, D.I., Eds.; Society of Economic Geologists, INC: Littleton, CO, USA, 1989; pp. 328–341.
77. Cook, N.J.; Chryssoulis, S.L. Concentrations of “invisible gold” in the common sulfides. *Can. Mineral.* **1990**, *28*, 1–16.
78. Fleet, M.E.; Mumin, H. Gold-bearing arsenian pyrite and marcasite and arsenopyrite from Carlin Trend gold deposits and laboratory synthesis. *Am. Mineral.* **1997**, *82*, 182–193. [[CrossRef](#)]
79. Genkin, A.D.; Bortnikov, N.S.; Cabri, L.J.; Wagner, F.E.; Stanley, C.J.; Safonov, Y.G.; McMahon, G.; Friedl, J.; Kerzin, A.L.; Gamyranin, G.N. A multidisciplinary study of invisible gold in arsenopyrite from four mesothermal gold deposits in Siberia, Russian Federation. *Econ. Geol.* **1998**, *93*, 463–487. [[CrossRef](#)]

80. Simon, G.; Kesler, S.E.; Chryssoulis, S. Geochemistry and textures of gold-bearing arsenian pyrite, Twin Creeks, Nevada: Implications for deposition of gold in Carlin-type deposits. *Econ. Geol.* **1999**, *94*, 405–422. [[CrossRef](#)]
81. Simon, G.; Huang, H.; Penner-Hahn, J.E.; Kesler, S.E.; Kao, L. Oxidation state of gold and arsenic in gold-bearing arsenian pyrite. *Am. Miner.* **1999**, *84*, 1071–1079. [[CrossRef](#)]
82. Stefansson, A.; Seward, T.M. Stability of chloride gold(I) complexes in aqueous solutions from 300 to 600 °C and from 500 to 1800 bar. *Geochim. Cosmochim. Acta* **2003**, *67*, 4559–4576. [[CrossRef](#)]
83. Benning, L.G.; Seward, T.M. Hydrosulphide complexing of Au(I) in hydrothermal solutions from 150–400 °C to 500–1500 bar. *Geochim. Cosmochim. Acta* **1996**, *60*, 1849–1871. [[CrossRef](#)]
84. Seward, T.M. Thio complexes of gold and the transport of gold in hydrothermal ore solutions. *Geochim. Cosmochim. Acta* **1973**, *37*, 370–399. [[CrossRef](#)]
85. Kesler, S.E.; Fortuna, J.; Ye, Z.J.; Alt, J.C.; Zohar, D.P.; Borhauer, J.; Chryssoulis, S.L. Evaluation of the role of sulfidation in deposition of gold, Screamer section of the Betze-Post Carlin-type deposit, Nevada. *Econ. Geol.* **2003**, *98*, 1137–1157. [[CrossRef](#)]
86. Li, T.; Ni, S.B. Element abundances of the continental lithosphere in China. *Geol. Prospectus* **1997**, *1*, 31–37.
87. Wu, Z.H.; Li, Z.Q.; Shi, Y.H.; Xiong, C.; Yang, H. Ore-controlling structure and prospecting direction of Zhesang glod deposit in Yunnan Province. *Metal Mine* **2014**, *1*, 95–99 (In Chinese with English abstract).
88. Yan, J.; Xia, Y.; Tan, Q.; Wang, Z.P.; Xie, Z.J.; Wang, J.T.; Zhang, H.X. Geological and Geochemistry Characteristics and Metallogenic Prediction of Carlin-type Gold Deposit in the Southeast Margin of Laizishan Anticline, Southwest of Guizhou Province. *Gold Sci. Technol.* **2015**, *23*, 28–37.
89. Naito, K.; Fukahori, Y.; He, P.M.; Sakurai, W.; Shimazaki, H.; Matsuhisa, Y. Oxygen and carbon isotope zonations of wall rocks around the Kamioka Pb-Zn skarn deposits, central Japan: Application to prospecting. *J. Geochem. Explor.* **1995**, *3*, 199–211. [[CrossRef](#)]
90. Vazquez, R.; Vennemann, T.W.; Kesler, S.E.; Russell, N. Carbon and oxygen isotope halos in the host limestone, El Mochito Zn-Pb-(Ag) skarn massive sulfide-oxide deposit, Honduras. *Econ. Geol.* **1998**, *1*, 15–31. [[CrossRef](#)]
91. Large, R.R.; Bull, S.W.; Winefield, P.R. Carbon and oxygen isotope halo in carbonates related to the McArthur River (HYC) Zn-Pb-Ag deposit, north Australia: Implications for sedimentation, ore genesis, and mineral exploration. *Econ. Geol.* **2001**, *7*, 1567–1593. [[CrossRef](#)]
92. Bierlein, F.P.; Arne, D.C.; Cartwright, I. Stable isotope (C, O, S) systematics in alteration haloes associated with orogenic gold mineralization in the Victorian gold province, SE Australia. *Geochem. Explor. Environ. Anal.* **2004**, *3*, 191–211. [[CrossRef](#)]
93. Kelley, D.L.; Kelley, K.D.; Coker, W.B.; Caughlin, B.; Doherty, M.E. Beyond the obvious limits of ore deposits: The use of mineralogical, geochemical, and biological features for the remote detection of mineralization. *Econ. Geol.* **2006**, *4*, 729–752. [[CrossRef](#)]
94. Ilchik, R.P. Geology and geochemistry of the Vantage gold deposits, Alligator Ridge-Bald Mountain mining district, Nevada. *Econ. Geol.* **1990**, *1*, 50–75. [[CrossRef](#)]
95. Stenger, D.P.; Kesler, S.E.; Vennemann, T. Carbon and oxygen isotope zoning around Carlin-type gold deposits: A reconnaissance survey at Twin Creeks, Nevada. *J. Geochem. Explor.* **1998**, *2*, 105–121. [[CrossRef](#)]
96. Arehart, G.B.; Donelick, R.A. Thermal and isotopic profiling of the Pipeline hydrothermal system: Application to exploration for Carlin-type gold deposits. *J. Geochem. Explor.* **2006**, *91*, 27–40. [[CrossRef](#)]
97. Hickey, K.A.; Ahmed, A.D.; Barker, S.L.; Leonardson, R. Fault-controlled lateral fluid flow underneath and into a Carlin-type gold deposit: Isotopic and geochemical footprints. *Econ. Geol.* **2014**, *5*, 1431–1460. [[CrossRef](#)]
98. Barker, S.L.L.; Dipple, G.M.; Hickey, K.A.; Lepore, W.A.; Vaughan, J.R. Applying stable isotopes to mineral exploration: Teaching an old dog new tricks. *Econ. Geol.* **2013**, *1*, 1–9. [[CrossRef](#)]
99. Vaughan, J.R.; Hickey, K.A.; Barker, S.L.L. Isotopic, chemical, and textural evidence for pervasive calcite dissolution and precipitation accompanying hydrothermal fluid flow in low-temperature, carbonate-hosted, gold systems. *Econ. Geol.* **2016**, *5*, 1127–1157. [[CrossRef](#)]

